Final Draft

of the original manuscript

Mülmenstädt, J.; Salzmann, M.; Kay, J.; Zelinka, M.; Ma, P.; Nam, C.; Kretzschmar, J.; Hörnig, S.; Quaas, J.:

An underestimated negative cloud feedback from cloud lifetime changes.

In: Nature Climate Change. Vol. 11 (2021) 6, 508 - 513.

First published online by Nature Publishing Group: 03.06.2021

https://dx.doi.org/10.1038/s41558-021-01038-1

An underestimated negative cloud feedback from cloud lifetime changes

Authors: Johannes Mülmenstädt,[1,2] Marc Salzmann,[1] Jennifer E. Kay,[3] Mark D. Zelinka[4], Po–Lun Ma[2], Christine Nam[1,*], Jan Kretzschmar[1], Sabine Hörnig[1], and Johannes Quaas[1]

[1]Institute for Meteorology, Universität Leipzig, Leipzig, Germany

[2]Atmospheric Sciences & Global Change Division, Pacific Northwest National Laboratory, Richland, Washington, USA

[3]Dept. of Atmospheric and Oceanic Sciences and Cooperative Institute for Research in Environmental Sciences, University of Colorado Boulder, Boulder, Colorado, USA

[4]Cloud Processes Research and Modeling Group, Lawrence Livermore National Laboratory, Livermore, California, USA

[*]now at Climate Services Center Germany, Hamburg, Germany

Abstract: As the atmosphere warms, part of the cloud population shifts from ice and mixed-phase ("cold") to liquid ("warm") clouds. Because warm clouds are more reflective and longer-lived, this phase change reduces the solar flux absorbed by Earth and constitutes a negative radiative feedback. This cooling feedback is weaker in CMIP6 than in CMIP5, contributing to greater greenhouse warming. While this change is often attributed to improvements in simulated cloud phase, another model bias persists: warm clouds precipitate too readily, potentially leading to underestimated negative lifetime feedbacks. Here we modify a climate model to better simulate warm rain probability and find it exhibits a cloud lifetime feedback nearly

three times larger than the default model. This suggests model errors in cloud-precipitation processes may bias cloud feedbacks as much as CMIP5–CMIP6 climate sensitivity differences. Reliable climate model projections therefore require improved cloud process realism guided by process-oriented observations and observational constraints.

Introduction

All aspects of the climate change problem hinge on knowing how sensitively the climate system will respond to a given anthropogenic perturbation to Earth's energy budget[1,2]. The largest uncertainty in estimates of climate sensitivity stems from the response of clouds to global warming[3–5], quantified as the "cloud feedback", i.e., a cloud-mediated feedback of the surface temperature increase onto the radiative energy imbalance of the climate system[6]. Recently, the sixth phase of the Coupled Model Intercomparison Project (CMIP6)[7] has yielded a higher multimodel-mean climate sensitivity estimate than previous assessments, in large part because the feedback due to extratropical low-altitude clouds has become less negative[5].

Extratropical low-cloud feedbacks arise from multiple mechanisms[8–10]: enhanced condensation[11,12]; enhanced evaporation[8,10,13,14]; and phase change as a part of the cloud population shifts from "cold" clouds (those containing ice or a mixture of ice and liquid) to "warm" clouds (those containing only liquid) in a warmer atmosphere[15,16]. The phase change feedback, in turn, is the sum of two components. First, because liquid water cloud droplets are typically smaller than ice particles and therefore have a higher surface area to volume ratio, liquid clouds are more reflective than ice clouds at the same vertically integrated condensate amount. We refer to this as the "optics component" of the phase feedback. Second, precipitation from warm clouds is inefficient compared to precipitation from cold clouds[15–18]. As a result, more warm clouds in the warmer atmosphere lead to a longer average residence time or "lifetime" of cloud condensate in the atmosphere, manifesting as a higher temporal-average condensate amount and thus a greater planetary albedo. We refer to this as the "lifetime component" of the phase

feedback by analogy to the "lifetime effect" in aerosol–cloud interactions[19,20], where lifetime is used metaphorically to comprise larger liquid water path and larger horizontal extent of clouds in addition to longer temporal extent.

Phase changes in midlatitude low-altitude clouds, especially over the Southern Ocean, constitute a particularly worrisome feedback mechanism because general circulation models (GCMs) have historically underestimated the fraction of supercooled liquid-topped clouds, leading to an underestimate of their albedo[21–27]. While this model error can be compensated by other model errors to allow models to meet their evaluation targets, it biases model estimates of the cloud response to warming because the present-day state contains too much cloud ice that is susceptible to replacement by liquid in a warmer atmosphere[28–31]. Between the fifth CMIP phase (CMIP5)[32] and CMIP6, many models have improved their representation of midlatitude clouds, increasing their supercooled liquid fraction. It is therefore tempting to conclude that the higher climate sensitivity in CMIP6 is a more physically plausible estimate of the true climate sensitivity.

Yet, many longstanding model errors remain unaddressed. Here we concentrate on errors in precipitation initiation in warm clouds. Using appropriately chosen precipitation statistics from spaceborne active remote sensing, we are able to place an observational constraint on the warm rain cloud process. We argue that this single-process constraint is a less uncertain constraint on climate projections than the more commonly performed observational constraints on cloud state, which are confounded by compensating errors among multiple processes with different sensitivities to anthropogenic perturbations. The warm rain process errors investigated here are widespread in climate models and were not systematically mitigated during CMIP6 development. We show that these errors bias model estimates of the midlatitude phase feedback to be *less* negative, in contrast to the errors in supercooled liquid cloud fraction which were mitigated in numerous models. In the ECHAM–HAMMOZ model used here, the phase feedback bias is of the same order of magnitude as the CMIP5-to-CMIP6 multimodel-mean feedback increase. Our results illustrate that observationally constraining the representation not only of

the cloud state but also of cloud processes in climate models is a necessary step towards reliable climate projections.

Results

We use fixed sea surface temperature (SST) simulations, an established experimental protocol for quantifying cloud feedbacks. Specifically, we evaluate the climate response to an idealized surface warming of 4 K by comparing atmospheric properties and radiative fluxes between a simulation with SST fixed to present-day climatology and a simulation with SST fixed to present-day climatology + 4 K[33] (see Methods) in ECHAM–HAMMOZ, a state-of-the-art atmospheric GCM[34]. We decompose the cloud phase feedback into an optics contribution λ_o and a lifetime contribution λ_ℓ by performing partial radiative perturbations (PRP; see Methods)[35–39]. The optics component results from a PRP application where the total condensate path is unperturbed but the cloud phase is perturbed, i.e., the vertical profiles of liquid and ice condensate mass fractions from the perturbed run are combined with the condensate mixing ratio profiles from the unperturbed run. The lifetime component results from a PRP application where the cloud phase is unperturbed but the total condensate amount is perturbed, i.e., the converse of the optics PRP application.

Our decomposition is shown as a function of latitude in Fig. 1 for the standard model configuration (Reference) and for a sensitivity run (described below). Feedbacks unrelated to phase change, such as drying through increased static stability, affect condensate amount globally and act as confounders in this decomposition; these feedbacks cause the strongly positive condensate path feedback seen in the lower latitudes in Fig. 1. The phase-change signals emerge in the mid-latitudes as local minima in the feedback strength near 60° latitude, especially in the southern hemisphere. We interpolate between the tropical and polar values of the feedback components and interpret the difference between the midlatitude local minima and the interpolation as the amplitude of the phase feedback components (see Methods). The global-mean lifetime feedback

is 2.4 times as strong as the optics feedback in this model by $\lambda_\ell = -0.059 \pm 0.015$ W m^{-2} K^{-1} to $\lambda_o = -0.025 \pm 0.005$ W m^{-2} K^{-1}. Our analysis is the first to provide separate estimates of the lifetime and optics feedback components in a GCM.

Figure 2a shows the warm rain fraction f_{warm}, defined as the fraction of rain occurrences that are due solely to warm rain processes (see Methods), in the ECHAM–HAMMOZ model. Atmospheric warming causes f_{warm} to increase (Fig. 2b). The increase Δf_{warm} is especially pronounced in the southern hemisphere midlatitudes, where abundant precipitating low-level oceanic clouds move from cold (mostly mixed-phase) to warm precipitation processes. Warm rain is rare over land compared to ocean at the same latitude[40,41]; thus, the presence of land mutes the corresponding northern hemisphere midlatitude signal.

GCMs with parameterized precipitation overestimate the propensity of warm clouds to rain[42–45]. This bias exists in the ECHAM–HAMMOZ model as well, shown in Fig. 3 as a bias in warm rain probability p_{warm}, defined as the probability of surface-reaching warm rain conditional on the presence of liquid-only cloud, relative to the satellite climatology of Mülmenstädt *et al.*[40]. As a result of this warm rain probability bias, we expect GCMs, including ECHAM–HAMMOZ, to overestimate the precipitation efficiency of warm clouds and thus underestimate the condensate lifetime increase as cold clouds transition to warm clouds. This implies an underestimate of the magnitude of the lifetime contribution to the cloud phase feedback. To test this hypothesis, we recalibrate the warm rain processes in ECHAM–HAMMOZ to better approximate the satellite-observed probability of warm rain in the present-day climate. Figure 3 shows the bias in p_{warm} in two configurations of the model: The "reference" configuration is the default model configuration; the "better average rain probability agreement with satellite" (BeARPAWS) configuration differs only in that we have artificially scaled the warm rain initiation process (parameterized as "autoconversion" of cloud water to rain water) so that the modeled p_{warm} better agrees with the satellite climatology (see Methods). Present-day liquid water path increases in the BeARPAWS configuration compared the reference model (Supplementary Figure 3), supporting our hypothesis that reducing p_{warm} decreases precipitation efficiency.

In accordance with our hypothesis, lower, more realistic warm rain probability leads to a more strongly negative cloud feedback via the condensate lifetime. Figure 1 shows a pronounced increase in the amplitude of the lifetime feedback near 60°S and the emergence of a northern hemisphere signal. Our estimate of the global-mean lifetime feedback in the warm rain bias-corrected model configuration is $\lambda'_\ell = -0.17 \pm 0.018$ W m^{-2} K^{-1} compared to $\lambda_\ell = -0.059 \pm 0.015$ W m^{-2} K^{-1} in the default configuration. Assessing the lifetime feedback in the bias-corrected model version incurs additional uncertainties because our strategy for recalibrating the warm rain process degrades the cloud state, a choice that we discuss in more detail below. A thorough examination of the uncertainty (see Methods) shows that the lifetime feedback in BeARPAWS is robustly stronger than in the reference model, with $1.3 < \lambda'_\ell/\lambda_\ell < 2.9$ at 95% confidence.

BeARPAWS is a heavy-handed model recalibration that degrades model performance in a number of other aspects, including radiative energy balance. However, it serves our purpose of determining what the consequences would be for the model's simulated climate if we reduced the warm precipitation bias rather than improving the model for general purposes. As we discuss in the Methods, the large uncertainty on $\lambda'_\ell/\lambda_\ell$ is the price we pay for the focus on a single process and the resulting degraded base state. The alternative would require touching a number of other model parameters, which would make it difficult to attribute the change in feedbacks to one particular parameterized process[46] (see Methods).

Our uncertainty estimates are valid for this particular model and assume that warm rain processes are the only source of model error. What we actually want to predict is what the feedback estimate would be in an ensemble of models without process errors, which, as discussed in the Methods, introduces additional, unquantified uncertainty. Therefore, our results should by no means be interpreted as a quantitative correction to be applied to CMIP6 feedback estimates. Rather, they provide qualitative guidance that the increase in cloud feedback in CMIP6 could be countered to a significant extent in a future model ensemble in which both cloud and precipitation errors have been mitigated. We see two promising avenues by which this guidance could be made less

uncertain. We encourage the inclusion of more advanced precipitation metrics, such as radar simulator diagnostics for precipitation frequency[45,47], in future iterations of the Cloud Feedback Model Intercomparison Project (CFMIP) contribution to CMIP[48] and in model development efforts. Notably, this would allow us to test whether our ECHAM–HAMMOZ conclusions translate to other models. We also advocate the pursuit of perturbed physics ensembles and model emulators as a way to quantify the sensitivity of cloud feedbacks to model parameters[49]. These techniques may enable exploration of the competition and error compensation between the processes responsible for the extratropical phase feedback as well as permitting more rigorous partitioning of the cloud feedback into components due to individual processes.

Discussion

Relative to CMIP5, many CMIP6 models exhibit a weaker negative extratropical cloud optical depth feedback[5], likely due to a weakened optics effect arising from increased mean-state supercooled liquid cloud water fraction. Improving the present-day cloud state representation in models is no guarantee that the sensitivity of the models to anthropogenic perturbations will be improved, however. The reason present-day state alone is an insufficient constraint is that many different processes contribute to the model state, and thus many different combinations of process representations can lead to equally valid representations of the present-day state; but these process representations can all differ in their sensitivity to climate perturbations, yielding different cloud feedbacks. This general property of open systems, dubbed equifinality[50], is well appreciated in other areas of the geosciences, such as hydrology[51] and aerosol radiative forcing[52,53]. Its manifestation in the extratropical cloud feedback is evident in single-model perturbed physics ensembles such as the one described by Tsushima *et al.*[49], which shows that the set of model parameters controlling cloud radiative effect over the Southern Ocean is largely orthogonal to the set controlling cloud feedback.

Thus, we advocate a focus on constraining individual processes, as we have done in Mülmenstädt

et al.[54] in the context of aerosol–cloud interactions. While improving the representation of a single process is likely to degrade the modeled present-day state by exposing formerly compensated errors in other processes, the only way to achieve a reliable model is to root out compensating process errors as the availability of suitable observations, insights from process-scale modeling, and physical understanding improves. The importance of reducing process errors is underscored by our result, which shows that the feedback bias associated with errors in a single process could be of the same order of magnitude as the CMIP5-to-CMIP6 multimodel-mean feedback change due to improvement in cloud state.

Warm rain processes are the focus of this paper because spaceborne active remote sensing enables us to construct a close proxy to a process rate – a binary estimate of autoconversion occurrence in the satellite footprint. Aside from being maximally coarse-grained (binary instead of continuous), this is conceptually the ideal observational constraint on process parameterizations, as parameterizations also yield process rates. Other processes are less directly tractable observationally. It is nevertheless important to continue to improve their representation in models so that the balance of processes in models is correct. This is especially important because precipitation and evaporation processes – both sinks of cloud condensate – can compensate for each others' errors in the present day cloud state but have opposite responses to greenhouse gas-induced warming[12,14].

Our remarks on the importance of process constraints by no means negate the importance of better constraining the present-day state in models. Processes can only be faithfully represented if the underlying cloud state is faithfully represented. Particularly for Southern Ocean clouds, this is a problem with modeling, observational, and model-evaluation aspects. Condensation, precipitation, and evaporation processes appear to trade places as the largest term in the condensate budget between different cloud regimes[12,55–57]. The relevant regimes may differentiate clouds not only into frontal convective versus cold-sector shallow types[23,29] but also by their mesoscale properties, such as precipitating shallow cumulus versus nonprecipitating stratus or stratocumulus. More comprehensive sampling of Southern Ocean clouds by active remote

sensing is required for process understanding across cloud types, and could be provided by the Aerosol–Cloud Convection Precipitation mission[58] if its spaceborne cloud radar can resolve the near-surface snow or rain production in shallow clouds. On the modeling side, correct representation of these regimes depends on correct representation of subgrid variability, since the mesoscale cloud organization is beyond the resolved scale of current GCMs. Beyond the physical problem of representing subgrid variability, the technical problem of consistency between subgrid variability as seen by model parameterizations and by satellite simulators[59,60] also requires urgent attention to ensure that observational evaluation of models is scale- and definition-aware[45]. Furthermore, the importance of correct representation of state extends beyond the cloud state to the aerosol state, because microphysical processes depend on both aerosol state and cloud state. Our results and those of many previous studies[15,61–63] suggest that microphysical processes strongly control the cloud feedback. This means that models need to represent the cloud-relevant aerosol properties over the Southern Ocean – and their change with global warming – correctly[55,64–67]. This is currently not the case[67,68].

Thus, a great deal of work remains to be done before we can be confident in our estimates of the extratropical cloud feedback. This will require a community-wide effort on process parameterization, process observations, and on the tools required to derive observational constraints on parameterized processes. Until then, we should not consider the less negative feedback in CMIP6 to be the last word; one of the most egregious model errors, and one uniquely tractable by a process-based observational constraint, could well cancel the CMIP6 increase in less biased future models.

References

[1] Nordhaus, W. D., Popp, D., What is the value of scientific knowledge?: An application to global warming using the price model, *Energy Journal* **18**, 1–45 (1997).

[2] Hope, C., The $10 trillion value of better information about the transient climate response, *Phil. Trans. Royal Soc. A* **373**, 20140429 (2015), https://doi.org/10.1098/rsta.2014.0429.

[3] Dufresne, J.-L., Bony, S., An assessment of the primary sources of spread of global warming estimates from coupled atmosphere-ocean models, *J. Climate* **21**, 5135–5144 (2008), https://doi.org/10.1175/2008JCLI2239.1.

[4] Vial, J., Dufresne, J.-L., Bony, S., On the interpretation of inter-model spread in cmip5 climate sensitivity estimates, *Clim. Dynam.* **41**, 3339–3362 (2013), https://doi.org/10.1007/s00382-013-1725-9.

[5] Zelinka, M. D., *et al.*, Causes of higher climate sensitivity in cmip6 models, *Geophysical Research Letters* **47**, e2019GL085782 (2020), https://doi.org/10.1029/2019GL085782.

[6] Schneider, S., Cloudiness as a global climatic feedback mechanism - effects on radiation balance and surface-temperature of variations in cloudiness, *J. Atmos. Sci.* **29**, 1413–+ (1972), https://doi.org/10.1175/1520-0469(1972)029<1413:CAAGCF>2.0.CO;2.

[7] Eyring, V., *et al.*, Overview of the coupled model intercomparison project phase 6 (cmip6) experimental design and organization, *Geosci. Model Dev.* **9**, 1937–1958 (2016), https://doi.org/10.5194/gmd-9-1937-2016.

[8] Gordon, N. D., Klein, S. A., Low-cloud optical depth feedback in climate models, *J. Geophys. Res.* **119**, 6052–6065 (2014), https://doi.org/10.1002/2013JD021052.

[9] Terai, C. R., *et al.*, Mechanisms behind the extratropical stratiform low-cloud optical depth response to temperature in arm site observations, *J. Geophys. Res.* **124**, 2127–2147 (2019), https://doi.org/10.1029/2018JD029359.

[10] Tan, I., Oreopoulos, L., Cho, N., The role of thermodynamic phase shifts in cloud optical depth variations with temperature, *Geophys. Res. Lett.* **46**, 4502–4511 (2019), https://doi.org/10.1029/2018GL081590.

[11] Betts, A., Harshvardhan, Thermodynamic constraint on the cloud liquid water feedback in climate models, *J. Geophys. Res.* **92**, 8483–8485 (1987), https://doi.org/10.1029/JD092iD07p08483.

[12] McCoy, D. T., Field, P., Bodas-Salcedo, A., Elsaesser, G. S., Zelinka, M. D., A regime-oriented approach to observationally constraining extratropical shortwave cloud feedbacks, *J. Climate* pp. 1–55 (2020), https://doi.org/10.1175/JCLI-D-19-0987.1.

[13] Tselioudis, G., Rossow, W., Rind, D., Global patterns of cloud optical-thickness variation with temperature, *J. Climate* **5**, 1484–1497 (1992), https://doi.org/10.1175/1520-0442(1992)005<1484:GPOCOT>2.0.CO;2.

[14] Myers, T. A., *et al.*, *Nature Climate Change* (in revision).

[15] Mitchell, J., Senior, C., Ingram, W., Co2 and climate - a missing feedback, *Nature* **341**, 132–134 (1989), https://doi.org/10.1038/341132a0.

[16] Tsushima, Y., *et al.*, Importance of the mixed-phase cloud distribution in the control climate for assessing the response of clouds to carbon dioxide increase: a multi-model study, *Clim. Dynam.* **27**, 113–126 (2006), https://doi.org/10.1007/s00382-006-0127-7.

[17] Senior, C., Mitchell, J., Carbon-dioxide and climate - the impact of cloud parameterization, *J. Climate* **6**, 393–418 (1993), https://doi.org/10.1175/1520-0442(1993)006<0393:CDACTI>2.0.CO;2.

[18] Hoose, C., Lohmann, U., Bennartz, R., Croft, B., Lesins, G., Global simulations of aerosol processing in clouds, *Atmos. Chem. Phys.* **8**, 6939–6963 (2008), https://doi.org/10.5194/acp-8-6939-2008.

[19] Albrecht, B. A., Aerosols, cloud microphysics, and fractional cloudiness, *Science* **245**, 1227–1230 (1989).

[20] Stevens, B., Feingold, G., Untangling aerosol effects on clouds and precipitation in a buffered system, *Nature* **461**, 607–613 (2009), https://doi.org/10.1038/nature08281.

[21] Bodas-Salcedo, A., Williams, K. D., Field, P. R., Lock, A. P., The surface downwelling solar radiation surplus over the southern ocean in the met office model: The role of mid-latitude cyclone clouds, *J. Climate* **25**, 7467–7486 (2012), https://doi.org/10.1175/JCLI-D-11-00702.1.

[22] Cesana, G., Chepfer, H., Evaluation of the cloud thermodynamic phase in a climate model using calipso-goccp, *J. Geophys. Res.* **118**, 7922–7937 (2013), https://doi.org/10.1002/jgrd.50376.

[23] Bodas-Salcedo, A., *et al.*, Origins of the solar radiation biases over the southern ocean in cfmip2 models, *J. Climate* **27**, 41–56 (2014), https://doi.org/10.1175/JCLI-D-13-00169.1.

[24] Komurcu, M., *et al.*, Intercomparison of the cloud water phase among global climate models, *J. Geophys. Res.* **119**, 3372–3400 (2014), https://doi.org/10.1002/2013JD021119.

[25] Cesana, G., Waliser, D. E., Jiang, X., Li, J.-L. F., Multimodel evaluation of cloud phase transition using satellite and reanalysis data, *J. Geophys. Res.* **120**, 7871–7892 (2015), https://doi.org/10.1002/2014JD022932.

[26] Kay, J. E., *et al.*, Evaluating and improving cloud phase in the community atmosphere model version 5 using spaceborne lidar observations, *J. Geophys. Res.* **121**, 4162–4176 (2016), https://doi.org/10.1002/2015JD024699.

[27] Bodas-Salcedo, A., *et al.*, Large contribution of supercooled liquid clouds to the solar radiation budget of the southern ocean, *J. Climate* **29**, 4213–4228 (2016), https://doi.org/10.1175/JCLI-D-15-0564.1.

[28] Tan, I., Storelvmo, T., Zelinka, M. D., Observational constraints on mixed-phase clouds imply higher climate sensitivity, *Science* **352**, 224–227 (2016), https://doi.org/10.1126/science.aad5300.

[29] Bodas-Salcedo, A., Andrews, T., Karmalkar, A. V., Ringer, M. A., Cloud liquid water path and radiative feedbacks over the southern ocean, *Geophys. Res. Lett.* **43**, 10938–10946 (2016), https://doi.org/10.1002/2016GL070770.

[30] Terai, C. R., Klein, S. A., Zelinka, M. D., Constraining the low-cloud optical depth feedback at middle and high latitudes using satellite observations, *J. Geophys. Res.* **121**, 9696–9716 (2016), https://doi.org/10.1002/2016JD025233.

[31] Frey, W. R., Kay, J. E., The influence of extratropical cloud phase and amount feedbacks on climate sensitivity, *Clim. Dynam.* **50**, 3097–3116 (2018), https://doi.org/10.1007/s00382-017-3796-5.

[32] Taylor, K. E., Stouffer, R. J., Meehl, G. A., An overview of cmip5 and the experiment design, *Bull. Amer. Meteorol. Soc.* **93**, 485–498 (2012), https://doi.org/10.1175/BAMS-D-11-00094.1.

[33] Cess, R., Potter, G., A methodology for understanding and intercomparing atmospheric climate feedback processes in general-circulation models, *J. Geophys. Res.* **93**, 8305–8314 (1988), https://doi.org/10.1029/JD093iD07p08305.

[34] Neubauer, D., Lohmann, U., Hoose, C., Frontoso, M. G., Impact of the representation of marine stratocumulus clouds on the anthropogenic aerosol effect, *Atmos. Chem. Phys.* **14**, 11997–12022 (2014), https://doi.org/10.5194/acp-14-11997-2014.

[35] Wetherald, R., Manabe, S., Cloud feedback processes in a general-circulation model, *J. Atmos. Sci.* **45**, 1397–1415 (1988), https://doi.org/10.1175/1520-0469(1988)045<1397:CFPIAG>2.0.CO;2.

[36] Colman, R. A., McAvaney, B. J., A study of general circulation model climate feedbacks determined from perturbed sea surface temperature experiments, *J. Geophys. Res.* **102**, 19383–19402 (1997), https://doi.org/10.1029/97JD00206.

[37] Colman, R., A comparison of climate feedbacks in general circulation models, *Clim. Dynam.* **20**, 865–873 (2003), https://doi.org/10.1007/s00382-003-0310-z.

[38] Klocke, D., Quaas, J., Stevens, B., Assessment of different metrics for physical climate feedbacks, *Clim. Dyn.* **41**, 1173–1185 (2013), https://doi.org/10.1007/s00382-013-1757-1.

[39] Mülmenstädt, J., *et al.*, Separating radiative forcing by aerosol-cloud interactions and fast cloud adjustments in the echam-hammoz aerosol-climate model using the method of partial radiative perturbations, *Atmos. Chem. Phys.* **19**, 15415–15429 (2019), https://doi.org/10.5194/acp-19-15415-2019.

[40] Mülmenstädt, J., Sourdeval, O., Delanoë, J., Quaas, J., Frequency of occurrence of rain from liquid-, mixed-, and ice-phase clouds derived from a-train satellite retrievals, *Geophys. Res. Lett.* **42**, 6502–6509 (2015), https://doi.org/10.1002/2015GL064604.

[41] Field, P. R., Heymsfield, A. J., Importance of snow to global precipitation, *Geophys. Res. Lett.* **42**, 9512–9520 (2015), https://doi.org/10.1002/2015GL065497.

[42] Stephens, G. L., *et al.*, Dreary state of precipitation in global models, *J. Geophys. Res.* **115**, D24211 (2010), https://doi.org/10.1029/2010JD014532.

[43] Suzuki, K., *et al.*, Evaluation of the warm rain formation process in global models with satellite observations, *J. Atmos. Sci.* **72**, 3996–4014 (2015), https://doi.org/10.1175/JAS-D-14-0265.1.

[44] Jing, X., *et al.*, A multimodel study on warm precipitation biases in global models compared to satellite observations, *J. Geophys. Res.* **122**, 11806–11824 (2017), https://doi.org/10.1002/2017JD027310.

[45] Kay, J. E., *et al.*, Scale-aware and definition-aware evaluation of modeled near-surface precipitation frequency using cloudsat observations, *J. Geophys. Res.* **123**, 4294–4309 (2018), https://doi.org/10.1002/2017JD028213.

[46] Golaz, J.-C., *et al.*, Sensitivity of the aerosol indirect effect to subgrid variability in the cloud parameterization of the gfdl atmosphere general circulation model am3, *J. Climate* **24**, 3145–3160 (2011), https://doi.org/10.1175/2010JCLI3945.1.

[47] Michibata, T., Suzuki, K., Ogura, T., Jing, X., Incorporation of inline warm rain diagnostics into the cosp2 satellite simulator for process-oriented model evaluation, *Geosci. Model Dev.* **12**, 4297–4307 (2019), https://doi.org/10.5194/gmd-12-4297-2019.

[48] Webb, M. J., *et al.*, The cloud feedback model intercomparison project (cfmip) contribution to cmip6, *Geosci. Model Dev.* **10**, 359–384 (2017), https://doi.org/10.5194/gmd-10-359-2017.

[49] Tsushima, Y., Ringer, M. A., Martin, G. M., Rostron, J. W., Sexton, D. M. H., Investigating physical constraints on climate feedbacks using a perturbed parameter ensemble, *Clim. Dynam.* **55**, 1159–1185 (2020), https://doi.org/10.1007/s00382-020-05318-y.

[50] von Bertalanffy, L., The theory of open systems in physics and biology, *Science* **111**, 23–29 (1950), https://doi.org/10.1126/science.111.2872.23.

[51] Beven, K., Freer, J., Equifinality, data assimilation, and uncertainty estimation in mechanistic modelling of complex environmental systems using the glue methodology, *JOURNAL OF HYDROLOGY* **249**, 11–29 (2001), https://doi.org/10.1016/S0022-1694(01)00421-8.

[52] Lee, L. A., Reddington, C. L., Carslaw, K. S., On the relationship between aerosol model uncertainty and radiative forcing uncertainty, *Proc. Nat. Acad. Sci. USA* **113**, 5820–5827 (2016), https://doi.org/10.1073/pnas.1507050113.

[53] Regayre, L. A., *et al.*, Aerosol and physical atmosphere model parameters are both important sources of uncertainty in aerosol erf, *Atmos. Chem. Phys.* **18**, 9975–10006 (2018), https://doi.org/10.5194/acp-18-9975-2018.

[54] Mülmenstädt, J., *et al.*, Reducing the aerosol forcing uncertainty using observational constraints on warm rain processes, *Science Adv.* **6**, eaaz6433 (2020), https://doi.org/10.1126/sciadv.aaz6433.

[55] Chubb, T. H., Jensen, J. B., Siems, S. T., Manton, M. J., In situ observations of supercooled liquid clouds over the southern ocean during the hiaper pole-to-pole observation campaigns, *Geophys. Res. Lett.* **40**, 5280–5285 (2013), https://doi.org/10.1002/grl.50986.

[56] Mace, G. G., Protat, A., Clouds over the southern ocean as observed from the r/v investigator during capricorn. part i: Cloud occurrence and phase partitioning, *J. Appl. Meteorol. Clim.* **57**, 1783–1803 (2018), https://doi.org/10.1175/JAMC-D-17-0194.1.

[57] Mace, G. G., Protat, A., Clouds over the southern ocean as observed from the r/v investigator during capricorn. part ii: The properties of nonprecipitating stratocumulus, *J. Appl. Meteorol. Clim.* **57**, 1805–1823 (2018), https://doi.org/10.1175/JAMC-D-17-0195.1.

[58] National Academies of Sciences, Engineering, and Medicine, *Thriving on Our Changing Planet: A Decadal Strategy for Earth Observation from Space* (The National Academies Press, Washington, DC, 2018), https://doi.org/10.17226/24938.

[59] Thayer-Calder, K., *et al.*, A unified parameterization of clouds and turbulence using clubb and subcolumns in the community atmosphere model, *Geosci. Model Dev.* **8**, 3801–3821 (2015), https://doi.org/10.5194/gmd-8-3801-2015.

[60] Song, H., Zhang, Z., Ma, P.-L., Ghan, S., Wang, M., The importance of considering sub-grid cloud variability when using satellite observations to evaluate the cloud and precipitation simulations in climate models, *Geosci. Model Dev.* **11**, 3147–3158 (2018), https://doi.org/10.5194/gmd-11-3147-2018.

[61] Ceppi, P., Hartmann, D. L., Webb, M. J., Mechanisms of the negative shortwave cloud feedback in middle to high latitudes, *J. Climate* **29**, 139–157 (2016), https://doi.org/10.1175/JCLI-D-15-0327.1.

[62] Bodas-Salcedo, A., *et al.*, Strong dependence of atmospheric feedbacks on mixed-phase microphysics and aerosol-cloud interactions in hadgem3, *J. Adv. Model. Earth Syst.* **11**, 1735–1758 (2019), https://doi.org/10.1029/2019MS001688.

[63] Gettelman, A., *et al.*, High climate sensitivity in the community earth system model version 2 (cesm2), *Geophys. Res. Lett.* **46**, 8329–8337 (2019), https://doi.org/10.1029/2019GL083978.

[64] Christensen, M. W., Suzuki, K., Zambri, B., Stephens, G. L., Ship track observations of a reduced shortwave aerosol indirect effect in mixed-phase clouds, *Geophys. Res. Lett.* **41**, 6970–6977 (2014), https://doi.org/10.1002/2014GL061320.

[65] Mccoy, D. T., *et al.*, Natural aerosols explain seasonal and spatial patterns of southern ocean cloud albedo, *Science Adv.* **1**, e1500157 (2015), https://doi.org/10.1126/sciadv.1500157.

[66] McCluskey, C. S., *et al.*, Observations of ice nucleating particles over southern ocean waters, *Geophys. Res. Lett.* **45**, 11989–11997 (2018), https://doi.org/10.1029/2018GL079981.

[67] Vergara-Temprado, J., *et al.*, Strong control of southern ocean cloud reflectivity by ice-nucleating particles, *Proc. Nat. Acad. Sci. USA* **115**, 2687–2692 (2018), https://doi.org/10.1073/pnas.1721627115.

[68] McCoy, I. L., *et al.*, The hemispheric contrast in cloud microphysical properties constrains aerosol forcing, *Proc. Nat. Acad. Sci. USA* **117**, 18998–19006 (2020), https://doi.org/10.1073/pnas.1922502117.

[69] Stephens, G., *et al.*, Cloudsat and calipso within the a-train: Ten years of actively observing the earth system, *Bull. Amer. Meteorol. Soc.* **99**, 569–581 (2018), https://doi.org/10.1175/BAMS-D-16-0324.1.

[70] Stevens, B., *et al.*, Atmospheric component of the mpi-m earth system model: Echam6, *J. Adv. Model. Earth Syst.* **5**, 146–172 (2013), https://doi.org/10.1002/jame.20015.

[71] Raddatz, T. J., *et al.*, Will the tropical land biosphere dominate the climate-carbon cycle feedback during the twenty-first century?, *Clim. Dynam.* **29**, 565–574 (2007), https://doi.org/10.1007/s00382-007-0247-8.

[72] Stier, P., *et al.*, The aerosol-climate model echam5-ham, *Atmos. Chem. Phys.* **5**, 1125–1156 (2005), https://doi.org/10.5194/acp-5-1125-2005.

[73] Zhang, K., *et al.*, The global aerosol-climate model echam-ham, version 2: sensitivity to improvements in process representations, *Atmos. Chem. Phys.* **12**, 8911–8949 (2012), https://doi.org/10.5194/acp-12-8911-2012.

[74] Kinnison, D. E., *et al.*, Sensitivity of chemical tracers to meteorological parameters in the mozart-3 chemical transport model, *J. Geophys. Res.* **112**, D20302 (2007), https://doi.org/10.1029/2006JD007879.

[75] Lohmann, U., Roeckner, E., Design and performance of a new cloud microphysics scheme developed for the echam general circulation model, *Clim. Dynam.* **12**, 557–572 (1996), https://doi.org/10.1007/s003820050128.

[76] Lohmann, U., *et al.*, Cloud microphysics and aerosol indirect effects in the global climate model echam5-ham, *Atmos. Chem. Phys.* **7**, 3425–3446 (2007), https://doi.org/10.5194/acp-7-3425-2007.

[77] Lohmann, U., Hoose, C., Sensitivity studies of different aerosol indirect effects in mixed-phase clouds, *Atmos. Chem. Phys.* **9**, 8917–8934 (2009), https://doi.org/10.5194/acp-9-8917-2009.

[78] Tiedtke, M., A comprehensive mass flux scheme for cumulus parameterization in large-scale models, *Mon. Weather Rev.* **117**, 1779–1800 (1989), https://doi.org/10.1175/1520-0493(1989)117<1779:ACMFSF>2.0.CO;2.

[79] Khairoutdinov, M., Kogan, Y., A new cloud physics parameterization in a large-eddy simulation model of marine stratocumulus, *Mon. Weather Rev.* **128**, 229–243 (2000), https://doi.org/10.1175/1520-0493(2000)128<0229:ANCPPI>2.0.CO;2.

[80] Rotstayn, L. D., On the "tuning" of autoconversion parameterizations in climate models, *J. Geophys. Res.* **105**, 15495–15507 (2000), https://doi.org/10.1029/2000JD900129.

[81] Weber, T., Quaas, J., Incorporating the subgrid-scale variability of clouds in the autoconversion parameterization using a pdf-scheme, *J. Adv. Model. Earth Syst.* **4**, M11003 (2012), https://doi.org/10.1029/2012MS000156.

[82] Lebsock, M., Morrison, H., Gettelman, A., Microphysical implications of cloud-precipitation covariance derived from satellite remote sensing, *J. Geophys. Res.* **118**, 6521–6533 (2013), https://doi.org/10.1002/jgrd.50347.

[83] Boutle, I. A., Abel, S. J., Hill, P. G., Morcrette, C. J., Spatial variability of liquid cloud and rain: observations and microphysical effects, *Quart. J. Roy. Meteorol. Soc.* **140**, 583–594 (2014), https://doi.org/10.1002/qj.2140.

[84] Zhang, Z., *et al.*, Subgrid variations of the cloud water and droplet number concentration over the tropical ocean: satellite observations and implications for warm rain simulations in climate models, *Atmos. Chem. Phys.* **19**, 1077–1096 (2019), https://doi.org/10.5194/acp-19-1077-2019.

[85] Gates, W., Amip - the atmospheric model intercomparison project, *Bull. Amer. Meteorol. Soc.* **73**, 1962–1970 (1992), https://doi.org/10.1175/1520-0477(1992)073<1962:ATAMIP>2.0.CO;2.

[86] Gates, W. L., *et al.*, An overview of the results of the atmospheric model intercomparison project (amip i), *Bull. Amer. Meteorol. Soc.* **80**, 29–55 (1999), https://doi.org/10.1175/1520-0477(1999)080<0029:AOOTRO>2.0.CO;2.

[87] Hurrell, J. W., Hack, J. J., Shea, D., Caron, J. M., Rosinski, J., A new sea surface temperature and sea ice boundary dataset for the community atmosphere model, *J. Climate* **21**, 5145–5153 (2008), https://doi.org/10.1175/2008JCLI2292.1.

[88] Bodas-Salcedo, A., *et al.*, Cosp satellite simulation software for model assessment, *Bull. Amer. Meteorol. Soc.* **92**, 1023–1043 (2011), https://doi.org/10.1175/2011BAMS2856.1.

[89] Nam, C. C. W., Quaas, J., Evaluation of clouds and precipitation in the echam5 general circulation model using calipso and cloudsat satellite data, *J. Climate* **25**, 4975–4992 (2012), https://doi.org/10.1175/JCLI-D-11-00347.1.

[90] Haynes, J. M., Marchand, R. T., Luo, Z., Bodas-Salcedo, A., Stephens, G. L., A multipurpose radar simulation package: Quickbeam, *Bull. Amer. Meteorol. Soc.* **88**, 1723–+ (2007), https://doi.org/10.1175/BAMS-88-11-1723.

[91] Cleveland, W., Robust locally weighted regression and smoothing scatterplots, *JOURNAL OF THE AMERICAN STATISTICAL ASSOCIATION* **74**, 829–836 (1979), https://doi.org/10.2307/2286407.

[92] Michibata, T., Suzuki, K., Takemura, T., Snow-induced buffering in aerosol–cloud interactions, *Atmos. Chem. Phys.* **20**, 13771–13780 (2020), https://doi.org/10.5194/acp-20-13771-2020.

[93] Gettelman, A., Morrison, H., Terai, C. R., Wood, R., Microphysical process rates and global aerosol-cloud interactions, *Atmos. Chem. Phys.* **13**, 9855–9867 (2013), https://doi.org/10.5194/acp-13-9855-2013.

[94] Lohmann, U., Neubauer, D., The importance of mixed-phase and ice clouds for climate

sensitivity in the global aerosol-climate model echam6-ham2, *Atmos. Chem. Phys.* **18**, 8807–8828 (2018), https://doi.org/10.5194/acp-18-8807-2018.

[95] Loeb, N. G., *et al.*, Clouds and the earth's radiant energy system (ceres) energy balanced and filled (ebaf) top-of-atmosphere (toa) edition-4.0 data product, *J. Climate* **31**, 895–918 (2018), https://doi.org/10.1175/JCLI-D-17-0208.1.

[96] NASA/LARC/SD/ASDC, Ceres energy balanced and filled (ebaf) toa monthly means data in netcdf edition4.0 (2017), https://doi.org/10.5067/TERRA+AQUA/CERES/EBAF-TOA_L3B004.0.

[97] Elsaesser, G. S., *et al.*, The multisensor advanced climatology of liquid water path (maclwp), *J. Climate* **30**, 10193–10210 (2017), https://doi.org/10.1175/JCLI-D-16-0902.1.

[98] Elsaesser, G., O'Dell, C., Lebsock, M., Teixeira, J., Multisensor advanced climatology mean liquid water path diurnal cycle l3 monthly 1 degree x 1 degree v1 (2016), https://doi.org/10.5067/MEASURES/MACLWPD.

[99] Li, J.-L. F., *et al.*, An observationally based evaluation of cloud ice water in cmip3 and cmip5 gcms and contemporary reanalyses using contemporary satellite data, *J. Geophys. Res.* **117**, D16105 (2012), https://doi.org/10.1029/2012JD017640.

[100] Adler, R. F., *et al.*, The version-2 global precipitation climatology project (gpcp) monthly precipitation analysis (1979-present), *JOURNAL OF HYDROMETEOROLOGY* **4**, 1147–1167 (2003), https://doi.org/10.1175/1525-7541(2003)004<1147:TVGPCP>2.0.CO;2.

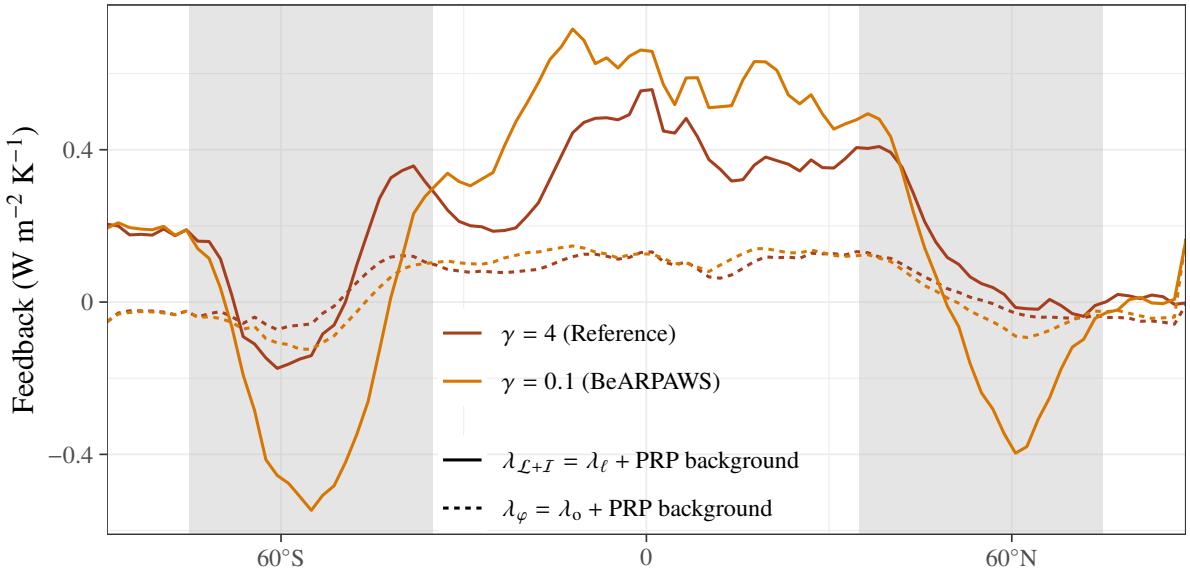

Figure 1: Zonal-mean feedback components. Feedbacks are computed by PRP in the reference and the BeARPAWS reduced warm rain probability configurations. PRP provides the sum of all feedback processes that change the total water path ($\lambda_{\mathcal{L}+\mathcal{I}}$) and cloud phase ($\lambda_\varphi$), respectively. A geographic fit (see Methods) is required to extract lifetime and optics feedbacks (λ_ℓ and λ_o) from $\lambda_{\mathcal{L}+\mathcal{I}}$ and λ_φ, respectively. Shading indicates the approximate regions in which λ_ℓ and λ_o produce a localized negative feedback distinguishable from the background of other feedback mechanisms (the background subtraction fit considers an ensemble of plausible geographic boundaries). Supplementary Figure 1 shows the background subtraction technique.

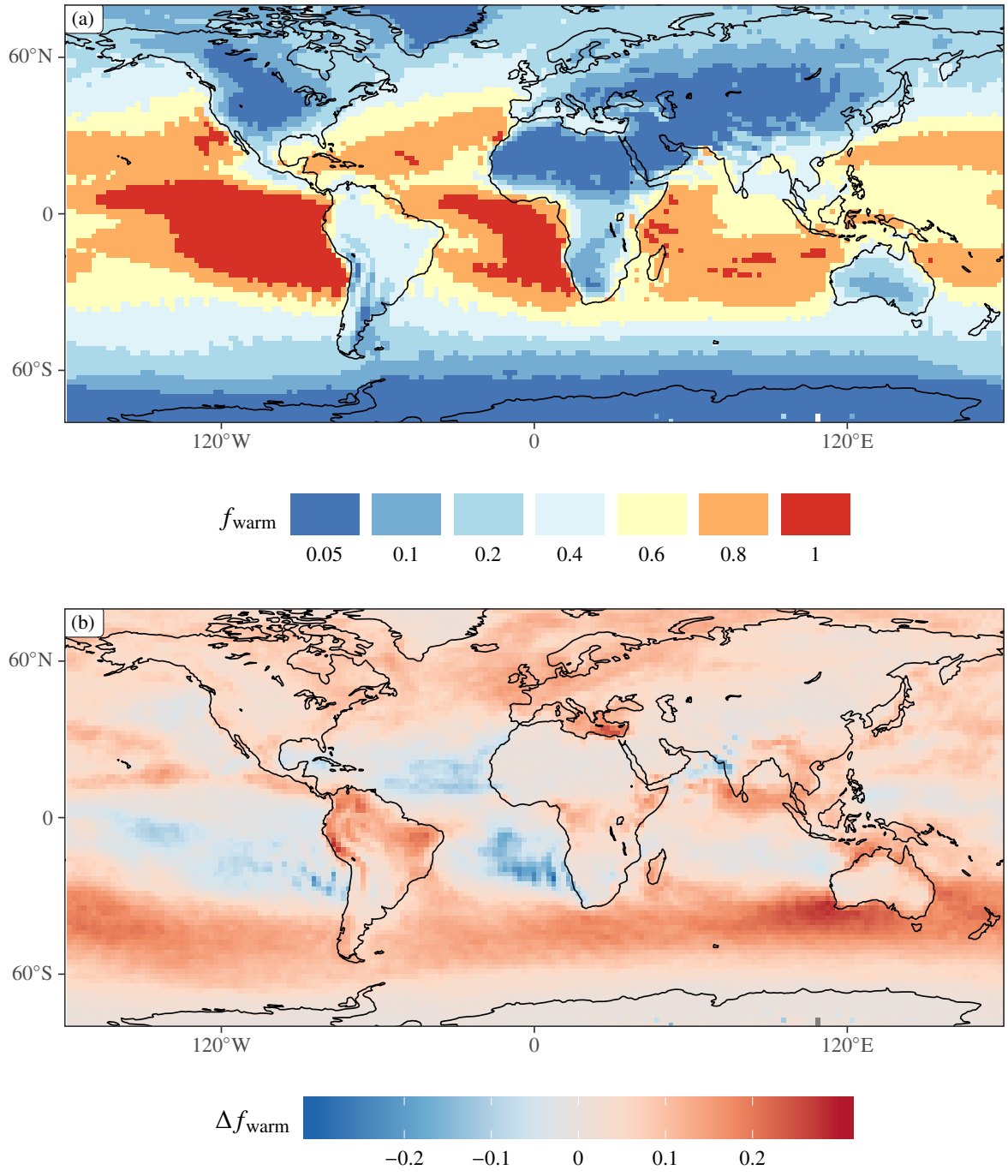

Figure 2: Warm rain fraction f_{warm} in the ECHAM–HAMMOZ model. Warm rain fraction in the simulation of the present-day climate is shown in panel (a). Warm rain fraction increase in a 4 K warmer climate relative to present day is shown in panel (b).

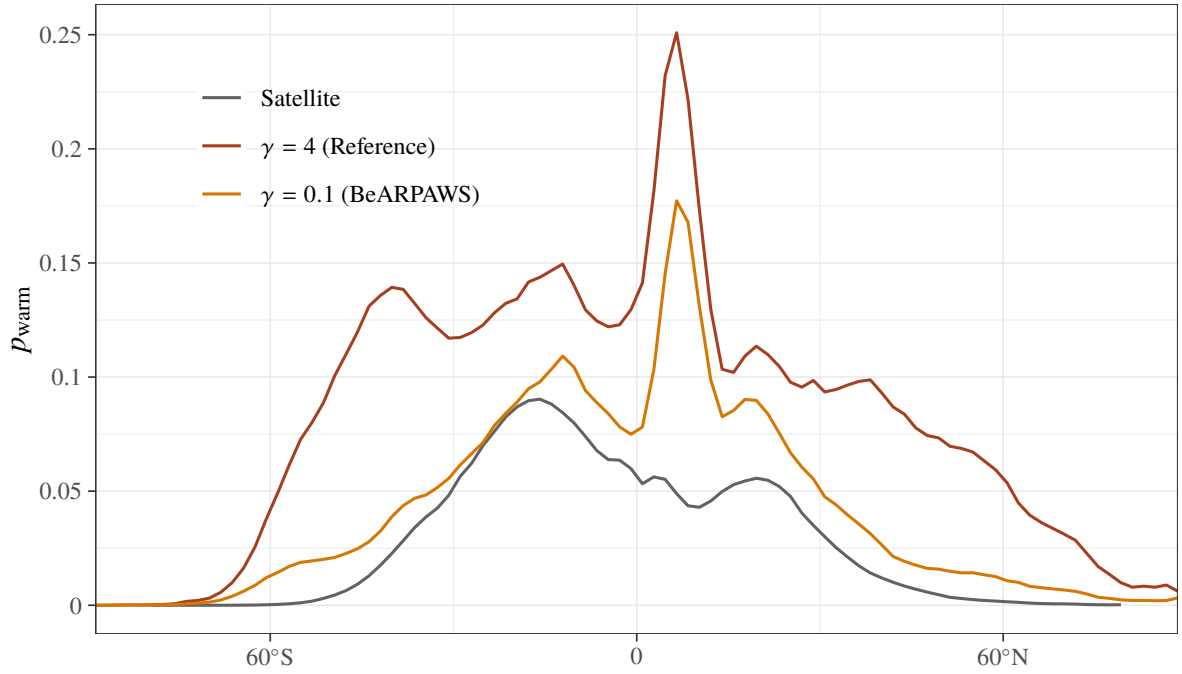

Figure 3: Zonal mean warm rain probability p_{warm}. The CloudSat–CALIPSO satellite climatology[40], reference model configuration, and BeARPAWS reduced warm rain model configuration are shown.

Methods

Observations of warm rain fraction and warm rain probability The observational dataset to which the model precipitation statistics are compared is the CloudSat–CALIPSO satellite radar–satellite lidar[69] warm/cold rain classification of Mülmenstädt *et al.*[40]. We use two fields from this climatology, described in greater detail in the reference. The warm rain fraction f_{warm} is defined as the temporal fractional occurrence of warm rain, normalized by the occurrence of any type of rain, within a grid box at latitude ϕ and longitude λ:

$$f_{\text{warm}}(\lambda, \phi) = \frac{n_{\text{warm rain}}(\lambda, \phi)}{n_{\text{warm rain}}(\lambda, \phi) + n_{\text{cold rain}}(\lambda, \phi)}. \tag{1}$$

The warm rain probability p_{warm} is the temporal fractional occurrence probability of warm rain conditional on the presence of warm cloud:

$$p_{\text{warm}}(\lambda, \phi) = \frac{n_{\text{warm rain}}(\lambda, \phi)}{n_{\text{warm cloud}}(\lambda, \phi)}. \tag{2}$$

In both equations (1) and (2), n_x refers to the number of CloudSat–CALIPSO profiles of type x. Using both f_{warm} and p_{warm} provides two complementary pieces of information about precipitation processes: f_{warm}, which is conditional on warm or cold precipitation occurrence, is the natural metric for ascertaining that precipitation processes shift from cold to warm in the warmer climate; whereas p_{warm}, which is a purely warm cloud derived metric, is the natural metric for evaluating warm rain processes specifically.

Atmospheric model We use ECHAM–HAMMOZ, version echam6.1–ham2.2–moz0.9[34], as a representative example of a state-of-the-art atmospheric GCM. ECHAM–HAMMOZ consists of the ECHAM6 atmospheric model[70], JSBACH land surface model[71], HAM aerosol module[72,73], and MOZART atmospheric chemistry module[74] (which we do not use in these model runs). Like GCMs in general, ECHAM–HAMMOZ represents precipitation both in its "convection" scheme and its large-scale ("stratiform") cloud scheme. The large-scale cloud

scheme consists of prognostic equations for cloud ice and water mixing ratio and particle number concentration with detailed treatment of liquid, mixed-phase, and ice precipitation formation processes[75–77], whereas the convective scheme[78] uses a cloud physics parameterization that makes it difficult to classify the thermodynamic phase of cloud and precipitation. We therefore only analyze cloud and precipitation thermodynamic phase in the large-scale cloud scheme. While the cloud and convection schemes parameterize very different atmospheric processes (large-scale ascent and subgrid-scale moist overturning, respectively), the partitioning of precipitation into large-scale and convective is largely arbitrary; in this model, precipitation in the midlatitudes is handled predominantly by the stratiform cloud scheme (see Supplementary Figure 3). This does not imply that the parameterized convection is inactive; detrainment from the convection is in fact a significant condensate source for the large-scale precipitation. It does, however, simplify our analysis by permitting us to focus on the large-scale precipitation parameterization.

Precipitation is treated diagnostically, i.e., precipitation is assumed to sediment out of the atmospheric column within one model time step (10 minutes). The rate at which the collision–coalescence "autoconversion" process converts cloud water into drizzle or rain water is parameterized based on the in-cloud droplet number concentration N_d and in-cloud liquid-water mixing ratio q_l as

$$\left.\frac{\partial q_l}{\partial t}\right|_{\text{aut}} = -1350\ \text{s}^{-1} \times \gamma q_l^{\alpha} \left(\frac{N_d}{1\ \text{cm}^{-3}}\right)^{-\beta} \tag{3}$$

[79]. The combination of parameters $\alpha = 2.47$, $\beta = 1.79$, and $\gamma = 1$ corresponds to the original Khairoutdinov and Kogan[79] parameterization for large eddy simulations. The ECHAM–HAMMOZ parameterization uses unchanged α and β parameters and $\gamma = 4$ to account for an enhancement of the autoconversion rate due to subgrid-scale variability[60,80–84]. Apart from this globally constant enhancement factor, no information on the subgrid-scale variability in N_d or q_l is available to the parameterization.

Present-day and future climate Model estimates of the cloud and precipitation response to global warming in this study are based on pairs of model runs. In each pair, one member represents the present-day climate and one represents the future, warmer climate. The runs require only an atmosphere and land surface model component. For the present day, we use an Atmospheric Model Intercomparison Project-derived (AMIP)[85–87] configuration (i.e., driven by the observed SST), updated monthly over the period 1992–2007. For the future climate, the model is run in the same configuration, except that we increase the AMIP SST by a constant 4 K. The strength of atmospheric feedbacks is given by the difference in top-of-atmosphere (TOA) fluxes between the two configurations divided by the surface temperature increase[33]. Among the advantages of this well established technique is that it permits feedbacks to be calculated for a model that is not in TOA energy balance.

Comparison of model and satellite warm rain statistics To enable scale- and definition-aware comparison between the model behavior and satellite retrievals[45], the CFMIP Observational Simulator Package (COSP)[88] has been implemented into ECHAM (updated to version 1.4.1 for the present study)[89]. Each model column is subdivided into 100 subcolumns; COSP then runs the QuickBeam[90] radar simulator to compute a radar reflectivity based on the hydrometeor mixing ratios and an assumed size distribution[89]. In ECHAM–HAMMOZ, the only subgrid-scale information passed to COSP is the vertical overlap assumption of fractional cloudiness. Hydrometeors are uniformly distributed throughout the cloudy part of the grid box. Model columns are counted as raining if their maximum radar reflectivity exceeds 0 dBZ_e and if the precipitation phase at the surface is liquid. If the highest cloud layer in which the reflectivity threshold is reached contains ice, the precipitation is classified as cold rain; otherwise, it is classified as warm rain. A cloud layer is defined as one or more vertically contiguous model levels with nonzero cloud condensate mixing ratio.

Calibrating warm rain probability The scale- and definition-aware evaluation of the modeled precipitation[45] thus accomplished can inform choices of the parameters in the autocon-

version formulation. We have chosen to use the enhancement factor γ from Equation (3) as our tuning parameter as a straightforward way to reduce the warm rain initiation rate and thus reduce p_{warm}. We showed in Mülmenstädt *et al.*[54] that the warm rain bias responds strongly to γ reductions, but that this strategy hits diminishing returns at $\gamma \approx 0.1$ without completely eliminating the bias. For this reason, we have chosen to use $\gamma = 0.1$ in this analysis, as well. Although reducing the autoconversion rate to achieve a more realistic warm rain representation is consistent with other analyses of advanced precipitation diagnostics[43], it clashes with the above-mentioned arguments that $\gamma > 1$ is required to account for subgrid-scale variability in precipitation processes. Our chosen model configuration therefore should not be seen as a "better" model in a general sense. There is no a priori justification for choosing $\gamma = 0.1$ (any more than there is for the reference configuration $\gamma = 4$); many other aspects of the model were calibrated to exist in harmony with the cloud and precipitation fields at $\gamma = 4$ and are now in disharmony with the new cloud and precipitation fields; and the $\gamma = 0.1$ model is out of energetic balance, precluding its use in a coupled ocean–atmosphere run. What we do expect this model configuration to be capable of, however, is to serve as a proxy for a model with reduced warm rain biases, so that we can use this configuration to draw inferences on the cloud phase feedback of a better model that may be many years in the future (or even unattainable).

With the exception of one sensitivity study described below, we explicitly choose not to tune any other aspect of the model to compensate for the TOA energy balance detuning introduced by the change in γ. The reason for this choice is that a tuning strategy involving more than one process makes it very difficult to attribute which of the process changes caused the change in emergent model properties, such as feedbacks or rapid adjustments[46,54].

Partial radiative perturbations to estimate radiative feedbacks To decompose the radiative feedback into the components of interest to us in this study, we use the method of partial radiative perturbations (PRP). PRP estimates the impact of a change in one property of the climate on the TOA radiative fluxes (and thus the total energy budget of the climate system) while holding all other properties fixed and is widely used for radiative feedback analysis[35–38].

The properties we perturb in this study are the cloud thermodynamic phase, holding total condensate path constant, to evaluate the optics component of the phase feedback; and the condensate path, holding thermodynamic phase constant, to evaluate the lifetime component of the phase feedback. Although one would expect large artifacts due to the decorrelation of highly correlated cloud properties when performing PRP on individual cloud properties, Mülmenstädt *et al.*[39] have demonstrated that it is possible to obtain accurate results by averaging between perturbing the AMIP run with an AMIP+4 K cloud property and perturbing the AMIP+4 K run with an AMIP cloud property (forward–backward PRP)[36].

A more formal description is given below, but the rather intuitive approach underlying the PRP-based feedback estimates is perhaps most clearly articulated in words. We archive the model cloud state every three hours in AMIP and AMIP+4 K model runs. After the runs complete, we then substitute cloud properties from one run into the output of the other run and recalculate radiative fluxes. This allows us to partition the total TOA radiative flux change resulting from the 4 K warming among changes in individual cloud variables. The individual cloud property changes we have considered are changes in total condensate holding cloud phase fixed; changes in cloud phase holding total condensate fixed; and fractional cloudiness. We have also substituted all cloud properties simultaneously (i.e., profiles of liquid and ice mixing ratios and fractional cloudiness) to ascertain that our decomposition sums to the full cloud feedback.

Adopting the notation of Mülmenstädt *et al.*[39], the vector of cloud properties relevant to the phase feedback in a two-moment homogeneous idealization of clouds is

$$\boldsymbol{x} = \{q_c, \varphi, N, f_c\}, \tag{4}$$

where q_c is the cloud condensate mixing ratio, N is the cloud particle number concentration, f_c is the fractional cloud coverage, and φ is the cloud thermodynamic phase. In the model, φ is encoded as the presence of ice or liquid through the separate liquid and ice-phase number

($\{N_d, N_i\}$) and mixing ratio ($\{q_l, q_i\}$) fields:

$$\boldsymbol{x} = \{q_l, q_i, N_d, N_i, f_c\}. \tag{5}$$

Denoting the AMIP run as A, AMIP+4 K run as B, and the TOA shortwave and longwave fluxes as Q and R, respectively, our goal is to determine the feedback parameters for the optical feedback (λ_o) and lifetime feedback (λ_ℓ). To do so, we first calculate the radiative effects of thermodynamic phase and condensate path:

$$\lambda_\varphi = \frac{1}{\Delta T_s}\overline{(\delta_{A\leftrightarrow B} Q_\varphi + \delta_{A\leftrightarrow B} R_\varphi)}, \tag{6}$$

$$\lambda_{\mathcal{L}+\mathcal{I}} = \frac{1}{\Delta T_s}\overline{(\delta_{A\leftrightarrow B} Q_{q_c} + \delta_{A\leftrightarrow B} R_{q_c})}, \tag{7}$$

where $\delta_{A\leftrightarrow B}\{Q, R\}_\xi$ denotes forward–backward PRP on cloud property ξ. To map between this conceptual operation and the actual model cloud properties, we proceed as follows. Rather than performing straightforward substitution of one cloud variable at a time, i.e.,

$$\boldsymbol{x} \mapsto \{x'_\xi, x_{\zeta\neq\xi}\} \tag{8}$$

(where run A provides the primed variable in the forward PRP case and run B provides the primed variable in the backward PRP case), we substitute both q_l and q_i at the same time:

$$\boldsymbol{x} \mapsto \{\hat{q}_l, \hat{q}_i, N_d, N_i, f_c\}, \tag{9}$$

where $\hat{q}_l, \hat{q}_i$ are functions of $\{q_l, q_i, q'_l, q'_i\}$, as described in detail below.

To determine $\lambda_{\mathcal{L}+\mathcal{I}}$, we apportion the *perturbed* condensate path according to the *unperturbed*

thermodynamic phase distribution:

$$\hat{q}_l = \begin{cases} q_l' + q_i' & \text{if } q_l \geq \varepsilon \text{ and } q_i < \varepsilon, \\ (q_l' + q_i')\dfrac{q_l}{q_l + q_i} & \text{if } q_l \geq \varepsilon \text{ and } q_i \geq \varepsilon, \\ 0 & \text{if } q_l < \varepsilon \text{ and } q_i \geq \varepsilon \end{cases} \tag{10}$$

and

$$\hat{q}_i = \begin{cases} 0 & \text{if } q_l \geq \varepsilon \text{ and } q_i < \varepsilon, \\ (q_l' + q_i')\dfrac{q_i}{q_l + q_i} & \text{if } q_l \geq \varepsilon \text{ and } q_i \geq \varepsilon, \\ q_l' + q_i' & \text{if } q_l < \varepsilon \text{ and } q_i \geq \varepsilon; \end{cases} \tag{11}$$

to determine λ_φ, we apportion the *unperturbed* condensate path according to the *perturbed* thermodynamic phase distribution:

$$\hat{q}_l = \begin{cases} q_l + q_i & \text{if } q_l' \geq \varepsilon \text{ and } q_i' < \varepsilon, \\ (q_l + q_i)\dfrac{q_l'}{q_l' + q_i'} & \text{if } q_l' \geq \varepsilon \text{ and } q_i' \geq \varepsilon, \\ 0 & \text{if } q_l' < \varepsilon \text{ and } q_i' \geq \varepsilon \end{cases} \tag{12}$$

and

$$\hat{q}_i = \begin{cases} 0 & \text{if } q_l' \geq \varepsilon \text{ and } q_i' < \varepsilon, \\ (q_l + q_i)\dfrac{q_i'}{q_l' + q_i'} & \text{if } q_l' \geq \varepsilon \text{ and } q_i' \geq \varepsilon, \\ q_l + q_i & \text{if } q_l' < \varepsilon \text{ and } q_i' \geq \varepsilon, \end{cases} \tag{13}$$

where $\varepsilon = 10^{-7}\ \mathrm{kg\,kg^{-1}}$ is the smallest mixing ratio that the model physics considers nonzero. As is often the case in physical systems, even a pleasantly symmetric set of governing equations such as equations (10–11) and (12–13) can yield very asymmetric numerical outcomes.

Although the ice crystal number concentration N_i is a prognostic variable in the cloud scheme, its effect on cloud optics is parameterized diagnostically as a function of q_i within the radiation scheme (eq. 7 in Stevens *et al.*[70]) via the ice effective radius

$$r_{e,i} = 83.8\,\mu\text{m} \times q_i^{0.216}. \tag{14}$$

For liquid clouds (and the liquid portion of mixed-phase clouds), we use the droplet number concentration N_d that corresponds to the thermodynamic phase distribution used in each radiative transfer calculation (i.e., $\hat{N}_d = N_d$ to calculate $\lambda_{\mathcal{L}+\mathcal{I}}$ and $\hat{N}_d = N'_d$ to calculate λ_φ). This prevents encounters with undefined droplet number when the substituted cloud field is purely ice. Mülmenstädt *et al.*[39] have shown that perturbing q_l and N_d independently is free of decorrelation artifacts.

To test that our decomposition closes, i.e., the sum of components equals the cloud feedback, we perform two additional PRP calculations. First, we calculate the fractional cloudiness feedback component λ_{f_c} by substituting f_c between the AMIP and AMIP+4 K runs:

$$\lambda_{f_c} = \frac{1}{\Delta T_s}\overline{(\delta_{A\leftrightarrow B} Q_{f_c} + \delta_{A\leftrightarrow B} R_{f_c})}; \tag{15}$$

second, we calculate the total cloud feedback λ_{cloud} by substituting the full set of cloud properties $\boldsymbol{x}$ from eq. (5):

$$\lambda_{\text{cloud}} = \frac{1}{\Delta T_s}\overline{(\delta_{A\leftrightarrow B} Q_{\boldsymbol{x}} + \delta_{A\leftrightarrow B} R_{\boldsymbol{x}})}. \tag{16}$$

As shown in Supplementary Figure 5, the decomposition closes well.

Differentiating between $\lambda_{\ell,\text{o}}$ and non-phase feedbacks Cloud feedbacks that are not mediated by phase change enter into the PRP-diagnosed λ_φ and (primarily) $\lambda_{\mathcal{L}+\mathcal{I}}$. Quantifying the phase feedback components $\lambda_{\ell,\text{o}}$ therefore requires a method to subtract the background of other feedbacks. Our technique is based on the distinctive geographic signature of the signal, which peaks slightly equatorward of 60° latitude. To estimate the background, we first make a best

guess at the signal-dominated region. We then fit a strongly smoothed local polynomial (locally estimated scatterplot smoothing, LOESS)[91] to the data excluding the signal region; this fit is our background estimate. Finally, we fit a normal distribution to the background-subtracted, area-weighted (i.e., $\cos\phi$-weighted) PRP output within the signal region; the integral of this fit is the global-mean feedback estimate. Supplementary Figure 1 illustrates the procedure. The method is purely phenomenological, i.e., the identification of the local minima with phase feedbacks is based on the assumption that there is no mechanism that would impart sharp latitudinal structure on other (evaporation-driven) feedback components over the midlatitudes. This assumption is supported to some extent by the geographical coincidence between the local minima in condensate feedback identified as the lifetime feedback signal on the one hand and the increase in warm rain fraction in the warmer climate on the other (see Supplementary Figure 2), as the transition to more warm rain is the hypothesized cause of the lifetime feedback. As we point out in the Discussion, the development of more rigorous methods for attributing feedback components to processes would be of great value, albeit made challenging by the interaction between processes.

The background subtraction technique has three uncertain parameters: the smoothing span s used in the background fit (as a fraction of the abscissa range) and the lower and upper latitude limits $\phi_{\min}$ and $\phi_{\max}$ of the signal region. To estimate the uncertainty associated with these parameter choices, we perform an ensemble of 10^4 fits with parameters uniformly and independently chosen from reasonable ranges: $0.65 \leq s \leq 0.8$, $35^\circ \leq |\phi_{\min}| \leq 45^\circ$, and $65^\circ \leq |\phi_{\max}| \leq 75^\circ$; these ranges are chosen to exclude unrealistic background models, where the fit connects the endpoints of the background region with a strongly concave-upward polynomial that overshoots near the poles (indicated by the dotted line in Supplementary Figure 1).

We choose to integrate the signal fit function rather than summing the background-subtracted PRP output because the fit function is well defined outside the signal region, so that the integral can be calculated over all latitudes. Summing the signal, by contrast, would be sensitive to the

width of the fit region or would require some other technique to extrapolate the signal into the background region.

Supplementary Table 1 summarizes the fit results and 95% confidence interval estimates for the fit components.

Quantifying feedback changes in an untuned model When we modify the γ factor in equation (3) to reduce the warm rain probability, the cloud state changes, primarily in that the liquid water path increases substantially (Supplementary Figures 3–4 and Supplementary Table 2). It is hard to imagine that this cloud state change would not affect the magnitude of the cloud feedback, and, indeed, all components of the cloud feedback are seen to respond to the changed base state in Supplementary Figure 5 and Supplementary Table 3. Our strategy of not compensating for the change in γ by retuning other model processes, while facilitating the attribution of the change in model behavior to the warm rain initiation process, thus requires us to perform additional analysis to ascertain that the increase in feedback strength is not due only to the increase in low cloud amount.

We seek to exclude the possibility that the increase in $|\lambda_\ell|$ follows entirely from the increase in low cloud amount after retuning the warm rain processes, rather than from having made the cloud lifetime more sensitive to ΔT_s. For concreteness, suppose that the feedback followed proportionally from the low cloud amount in the present-day climate; in that case, a model tuned to a higher present-day low cloud amount would appear to give a larger $|\lambda_\ell|$, but this larger $|\lambda_\ell|$ would not permit the conclusion that the GCM warm rain bias causes an underestimate of $|\lambda_\ell|$. In Supplementary Figure 6, we normalize the feedbacks by various measures of low cloud amount in the present-day climate simulation: liquid water path $\mathcal{L}$; shortwave cloud radiative effect $\mathcal{S}_c$; and λ_o (to test whether both feedback components simply show the same dependence on cloud state). In all cases, the normalized feedback λ_ℓ/χ, $\chi \in \{\mathcal{L}, \mathcal{S}_c, \lambda_\mathrm{o}\}$, is stronger in the model configuration with reduced warm rain probability. The lifetime feedback component also responds more strongly to the reduced warm rain probability than the optical feedback component. These outcomes are all consistent with our interpretation that the reduced warm

rain efficiency causes the increase in $|\lambda_\ell|$.

Further confidence comes from using the lower latitudes as a test of the ability of the method to distinguish between feedback strengthening due to process changes and feedback strengthening purely due to increased cloud in the base state. In the lower latitudes, the lifetime mechanism does not contribute to the cloud feedback, so any increase in feedback strength in BeARPAWS compared to the reference configuration is presumably due to the low cloud increase in the lower warm rain probability configuration. If the normalization method works as intended, the normalized feedback should be similar (or – if the normalization is conservative – lower) in BeARPAWS compared to the reference. Supplementary Figure 6 shows that BeARPAWS does indeed produce a stronger feedback in the lower latitudes which, upon normalization, becomes close to or weaker than in the reference simulation. This appears to work particularly well when normalizing by the shortwave cloud radiative effect, consistent with the reasonable hypothesis that radiative feedback strength in the absence of a process difference is simply proportional to radiative effect. Normalizing by $\mathcal{L}$, by contrast, appears overly conservative, which may perhaps be explained by radiative effects saturating at higher $\mathcal{L}$. Thus, the lower-latitude behavior of the feedbacks lends further support to the notion that normalizing the feedback allows us to determine when a feedback strengthening is purely the result of an increase in cloud amount.

Supplementary Table 4 summarizes the normalized feedback estimates. These estimates are derived using the background subtraction technique described above; the regional-average ratio is computed by averaging numerator and denominator before dividing. For $\chi \in \{\mathcal{S}_c, \mathcal{L}\}$, the denominator is the $\cos\phi$-weighted average over the signal region; for $\chi = \lambda_o$, the denominator is the result of the signal fit procedure applied to λ_o. The numerator is the result of the signal fit procedure applied to λ_ℓ in all cases.

We can similarly estimate the ratios of normalized feedbacks between the $\gamma = 4$ (reference) and $\gamma = 0.1$ (recalibrated warm rain probability) configurations. Depending on the choice of denominator, the lifetime feedback component is between 1.3 and 2.9 times as strong in the recalibrated warm rain probability configuration as in the default configuration. The set of

denominators we have considered includes all relevant cloud variables; we therefore estimate that this range corresponds to at least 95% coverage.

Finally, we can estimate the λ_ℓ/λ_o ratio. In either configuration, λ_ℓ is the dominant component of the phase feedback in this model.

Quantifying feedback changes when multiple processes are retuned to maintain the cloud state In addition to the normalized feedback ansatz, we have also performed an experiment where we tuned the lower warm rain probability model into a similar cloud state as the reference configuration. Reproducing the base state comes at the expense of tuning more than one process, complicating the interpretation of the model behavior and its attribution to individual processes.

To keep the retuning within the same sector of the model, we have chosen to modify accretion (collection of cloud droplets by rain drops), which is the other warm rain process parameterized in this model. In ECHAM–HAMMOZ, the accretion parameterization follows Khairoutdinov and Kogan[79]:

$$\left.\frac{\partial q_l}{\partial t}\right|_{\text{acc}} = -3.7\ \text{s}^{-1} \times \gamma_{\text{acc}} q_l q_r, \tag{17}$$

where q_r is the mixing ratio of rain water. Increasing the tuning factor for this process increases the efficiency of liquid condensate removal by both warm and cold rain. Employed in conjunction with the same reduced tuning factor for autoconversion as in the BeARPAWS configuration, a tenfold increase in the accretion tuning factor allows us to achieve the dual goals of reduced (albeit less strongly than BeARPAWS) warm rain probability (Supplementary Figure 8) and unchanged present-day liquid water path (Supplementary Figure 7). Compared to the reference configuration, this configuration is less likely to initiate warm rain, but once (warm or cold) rain occurs, the rain more efficiently removes cloud water. We refer to this configuration as "BeARPAWS energy and hydrology validation experiment" (BEAHyVE).

In the BEAHyVE configuration, p_{warm} (averaged over the same sampling of latitude ranges as the background subtraction fit) is biased high by 0.041 relative to the satellite estimate, while the lifetime feedback estimate is $\lambda_\ell = -0.084 \pm 0.007\ \text{W m}^{-2}\ \text{K}^{-1}$. Both the feedback estimate

and the p_{warm} bias reduction thus lie between the reference and BeARPAWS values. (The p_{warm} biases are 0.068 in the reference and 0.012 in the BeARPAWS configuration; the lifetime feedbacks are $-0.059\ \mathrm{W\,m^{-2}\,K^{-1}}$ in the reference and $-0.17\ \mathrm{W\,m^{-2}\,K^{-1}}$ in the BeARPAWS configuration.) Because the p_{warm} biases differ between BeARPAWS and BEAHyVE, comparing the lifetime feedback estimates introduces some ambiguity. Assuming, somewhat arbitrarily, that the feedback estimate would scale linearly if the BEAHyVE configuration were extensible to lower p_{warm} bias, we estimate $1.3 < \lambda'_\ell/\lambda_\ell < 3.0$ for the BEAHyVE lifetime feedback relative to the reference lifetime feedback at the BeARPAWS p_{warm} reduction. The upper and lower bounds are obtained by assuming either the absolute lifetime feedback or the lifetime feedback strengthening relative to the reference configuration scales with the warm rain probability, respectively. This range is consistent with the range obtained by the method of normalizing BeARPAWS to cloud state changes in the previous section.

Rain and snow water content are not prognostic variables in ECHAM–HAMMOZ, similar to the situation in many other GCMs[92]; precipitation is assumed to fall through the grid column within a model time step. This diagnostic treatment of precipitation is known to bias accretion low[93], which, along with enhancement due to subgrid-scale variability[83,84], provides some justification for a greater-than-unity accretion tuning factor. However, we stress that the tuning factor is too large to be compatible with these possible explanations (and requires an even more unrealistic autoconversion scale factor). In our opinion, the tuning strategy used, at best, masks structural deficiencies in the model. Therefore, our point about using BeARPAWS for guidance rather than as a model improvement applies even more strongly to BEAHyVE.

As may have been expected, extending the tuning strategy to two parameters results in more complex model behavior. Supplementary Figure 9 shows that the shape of the condensate feedback in BEAHyVE differs from both the reference configuration and BeARPAWS. The decreased autoconversion tuning factor in BeARPAWS appears to effect both an increase in the amplitude of the lifetime feedback in the SW spectrum and an equatorward broadening (Supplementary Figure 10). In the BEAHyVE configuration, in contrast, the lifetime feedback strength

increases only because of an equatorward broadening of the region across which the feedback operates, partially offset by a more strongly positive feedback in the LW spectrum everywhere. This illustrates the complications arising from multiparameter tuning strategies; while they are necessary if the present-day cloud state is to be maintained across model configurations, disentangling the mechanisms by which they affect climate projections is challenging.

Caveats on uncertainty estimates In the Results section, we pointed out that our uncertainty estimates are for the lifetime and optics feedback components in this particular model and assuming that warm rain processes are the only source of model error. This raises two caveats.

The first caveat concerns how representative of the CMIP ensemble the behavior of this model is. The strong lifetime feedback relative to the optical feedback is, so far, an ECHAM–HAMMOZ-specific result. This model has a low base-state supercooled liquid water fraction compared to other models[24]; based on Tan *et al.*[28], Terai *et al.*[30], Frey and Kay[31], we would expect ECHAM–HAMMOZ to overestimate the optical component of the phase feedback, but Lohmann and Neubauer[94] have shown the model to be insensitive to base state supercooled liquid fraction, making its optical component behavior somewhat unusual among GCMs. Its warm rain bias, however, is unremarkable compared to other models[43,44], leading us to expect the indicating lifetime component estimate to be fairly representative of other models. If this is the case, then our conclusion that the lifetime feedback dominates the total cloud phase feedback will hold in the multimodel mean, as well. Making this determination directly is currently not possible for the majority of CMIP models because the appropriate diagnostics, such as those of Michibata *et al.*[47], are too new to have been included in CMIP6. We encourage the inclusion of such diagnostics in future multimodel ensembles.

The second caveat, at its root, concerns the interaction between parameterizations in a complex model, including the interaction between errors within these parameterizations. Sources of uncertainty include the arbitrary partitioning of precipitation processes between "convective" and "stratiform" clouds with different levels of sophistication in their microphysics; errors in cloud representation that complicate the interpretation of the diagnostics we use in this study;

and compensation between precipitation and other model errors. In this study, we have only modified stratiform precipitation, which is the more detailed of the two parameterizations; this is unlikely to result in a large error in our $\lambda'_\ell/\lambda_\ell$ estimate, as most of the precipitation at the relevant latitudes is from the stratiform scheme in this model (see Supplementary Figure 3). The model does not represent subgrid-scale cloud variability (beyond fractional cloudiness within a grid cell). One consequence is that this limits the model's ability to capture mesoscale shallow cloud regimes (see Discussion). Another is that all clouds within a grid cell precipitate equally, which is not representative of the spatial variability in real clouds but paradoxically reduces the potential for misinterpreting evaluation errors (from communicating subgrid variability to the radar simulator) as model errors[59,60]. Finally, a hypothetical future model in which other compensating errors have already been addressed might require a less drastic retuning of warm rain processes. An otherwise perfect model would probably exhibit a smaller feedback bias because evaporation would be a more important and precipitation a less important sink process. A smaller warming-induced shift from cold to warm rain in a model that better represents supercooled liquid in shallow clouds may also reduce the bias, although incorrect phase assignment in the model may partially compensate for the importance of cold rain processes even in predominantly supercooled liquid clouds[55,56]. This source of uncertainty is very difficult to quantify, as it involves the interaction of components of a complex system. It does, however, highlight aspects of the model (and other models with similar errors) that urgently require improvement. We discuss these in the Discussion section.

Data availability: Summary data files of the model runs used in this article are available at DOI `https://doi.org/10.5281/zenodo.4587416`.

Code availability: The code that was used to perform model analysis and produce the figures and tables is freely available at DOI `https://doi.org/10.5281/zenodo.4603964`. The ECHAM–HAMMOZ model code is available at `https://hammoz.ethz.ch` subject to acknowledgment of a license; the modifications made for this analysis are freely available at DOI

https://doi.org/10.5281/zenodo.4604019.

Acknowledgments: The authors thank Chris Bretherton, Susannah Burrows, Steve Klein, Jay Mace, Daniel McCoy, Isabel McCoy, Christina Sackmann, Ivy Tan, Rob Wood, and three reviewers for their comments. The ECHAM–HAMMOZ model is developed by a consortium composed of ETH Zurich, Max Planck Institut für Meteorologie, Forschungszentrum Jülich, University of Oxford, the Finnish Meteorological Institute, and the Leibniz Institute for Tropospheric Research, and managed by the Center for Climate Systems Modeling (C2SM) at ETH Zurich. Computing resources were provided by Deutsches Klimarechenzentrum (DKRZ). Ice water path data was provided by Frank Li. GPCP data was provided by the NOAA/OAR/ESRL PSL, Boulder, Colorado, USA, from their Web site at https://psl.noaa.gov/. Public domain map data was provided by https://naturalearthdata.com. JM and JQ were supported by European Research Council (ERC) project "QUAERERE", grant agreement 306284. JM and PM were supported by the U.S. Department of Energy (DOE), Office of Science, Office of Biological and Environmental Research, Regional and Global Model Analysis Program. PM was supported by the Leibniz Invitations program at Universität Leipzig. JEK was supported by NSF CAREER AGS 1554659 and NASA Award 80NSSC20K0133. MZ's work was supported by the U.S. DOE Regional and Global Model Analysis Program and was performed under the auspices of the U.S. DOE under Contract DE-AC52-07NA27344. The work of JQ is supported by the European Union via its Horizon 2020 projects CONSTRAIN (GA 820829) and FORCeS (GA 821205). The Pacific Northwest National Laboratory is operated for the U.S. DOE by Battelle Memorial Institute under contract DE-AC05-76RL01830.

Author contributions: JM, MS, JEK designed the study; MDZ provided multimodel-mean results; CN, MS, JK, and JM implemented COSP into ECHAM–HAMMOZ; JM and SH performed simulations; all authors contributed to the interpretation of the model results; JM drafted the manuscript with contributions from all authors.

Conflicts of interest: The authors state that they have no conflicts of interest.

Additional information: **Supplementary Information** is available for this paper. Correspondence and requests for materials should be addressed to johannes.muelmenstaedt@pnnl.gov.

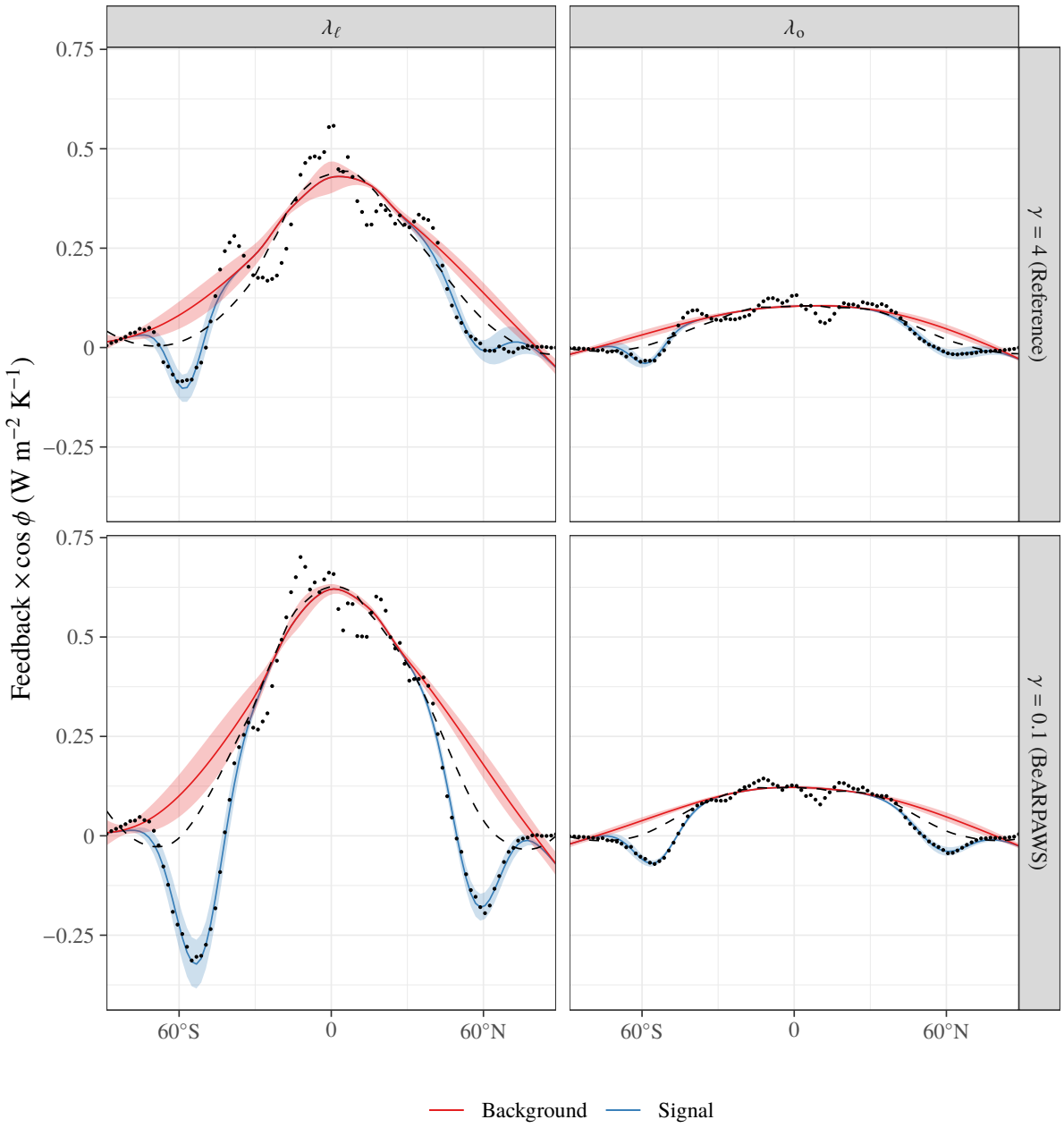

Supplementary Figure 1: Distinguishing between $\lambda_{\ell,o}$ and non-phase contributions to the cloud feedbacks. Zonal-mean PRP results are shown as points. The red band illustrates the 95% confidence interval of background models; the blue band illustrates the 95% confidence interval of signal models. The dashed line is an example of a poor background fit obtained with fit parameters outside the ranges given in the text ($s = 0.57$, $\phi_{min} = 36°$, $\phi_{max} = 61°$).

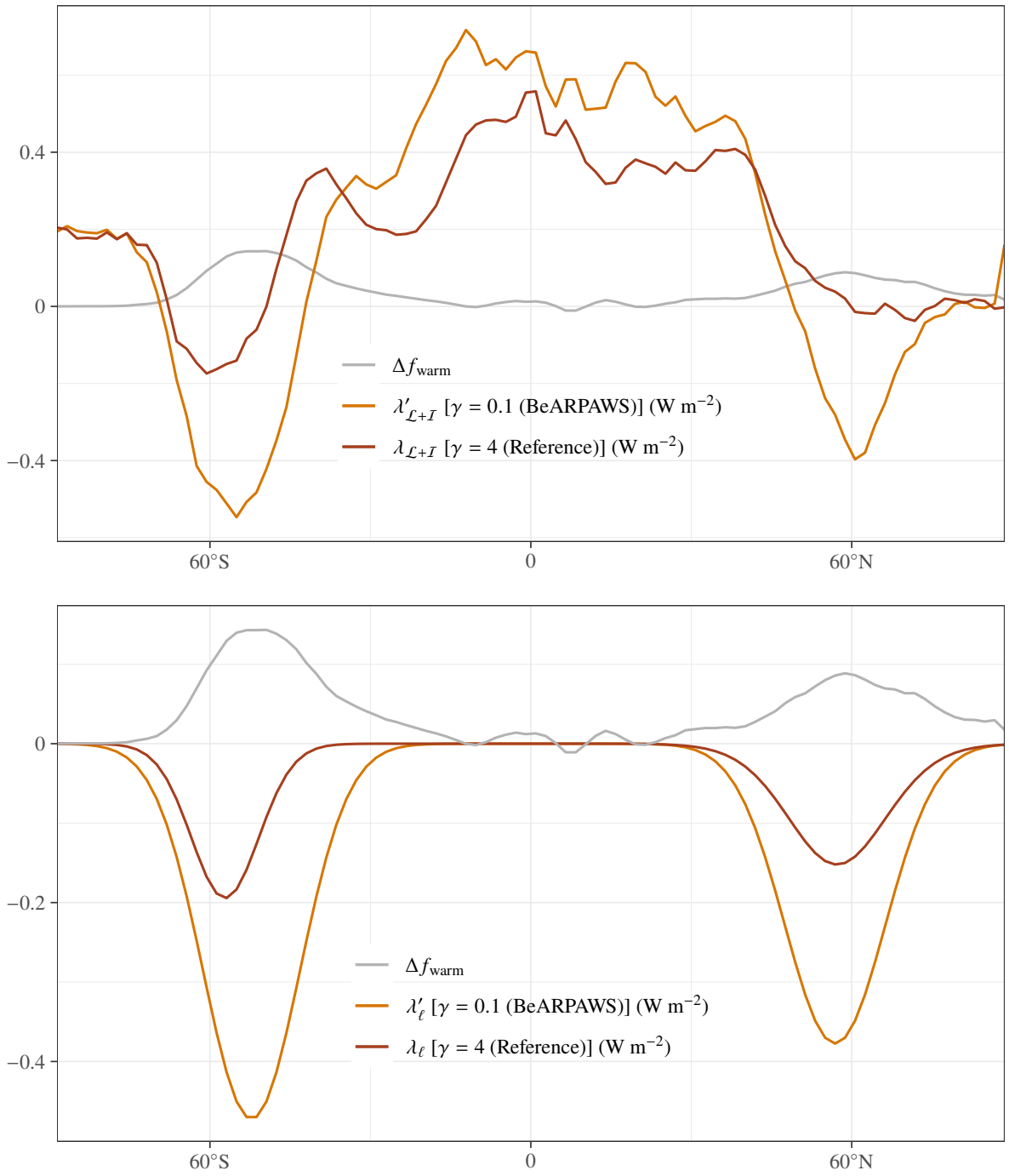

Supplementary Figure 2: Approximate geographic coincidence between change from cold to warm rain and cloud feedbacks. The condensate path feedback (top) and lifetime feedback signal (bottom) occur close to the latitudes of greatest increase in f_{warm}.

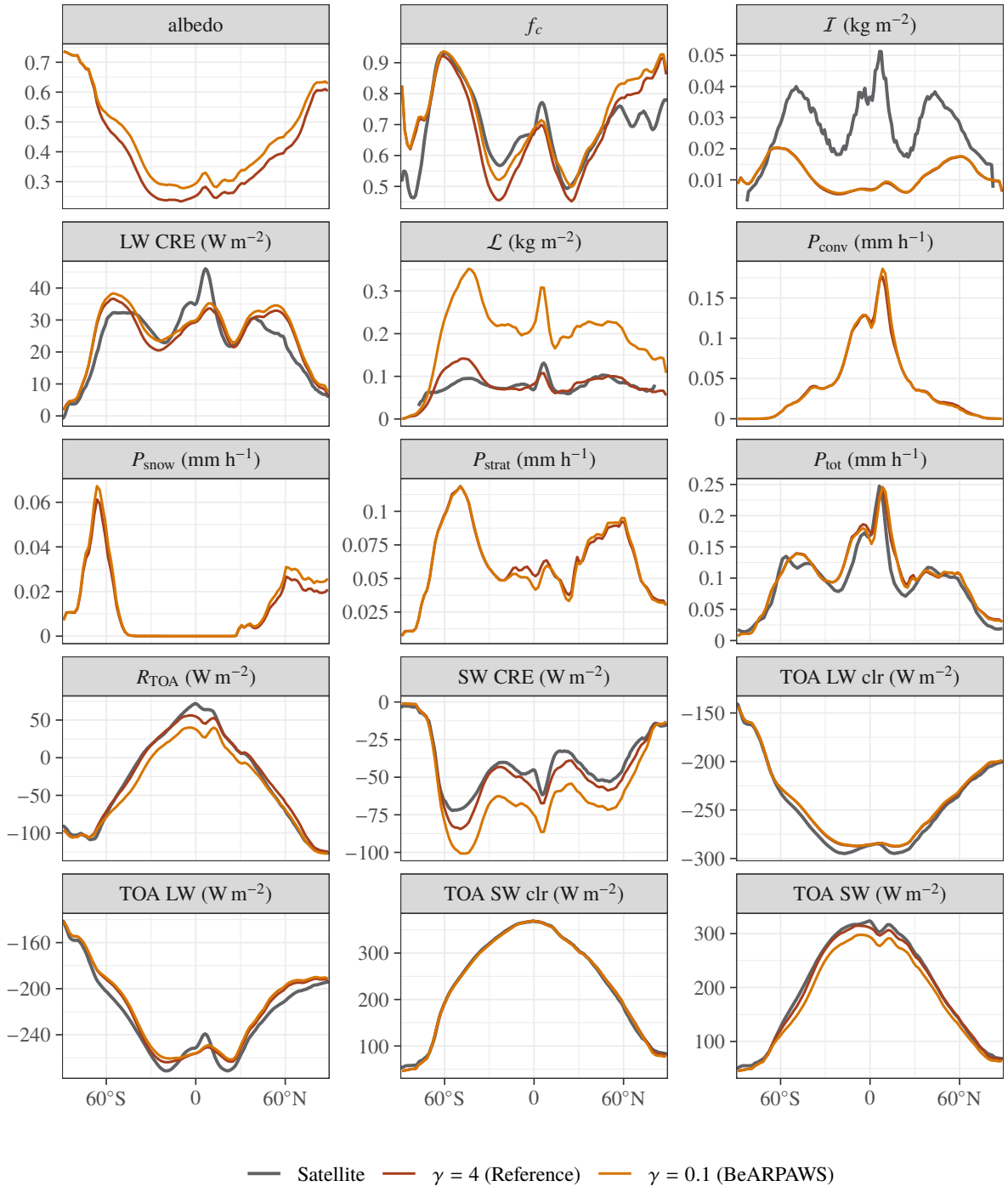

Supplementary Figure 3: Atmospheric state variables. The satellite products drawn for comparison are CERES–EBAF version 4.0[95,96] for radiative fluxes, cloud radiative effects, and f_c; MAC–LWP[97,98] for $\mathcal{L}$; CloudSat 2C-ICE following Li *et al.*[99] for for $\mathcal{I}$; and GCPC version 2.3[100] for precipitation. The reference and reduced autconversion (BeARPAWS) model configurations are shown.

Supplementary Figure 4: Atmospheric state variable changes in the warmer climate. The change from AMIP to AMIP+4 K is shown for the reference and reduced autconversion (BeARPAWS) model configurations.

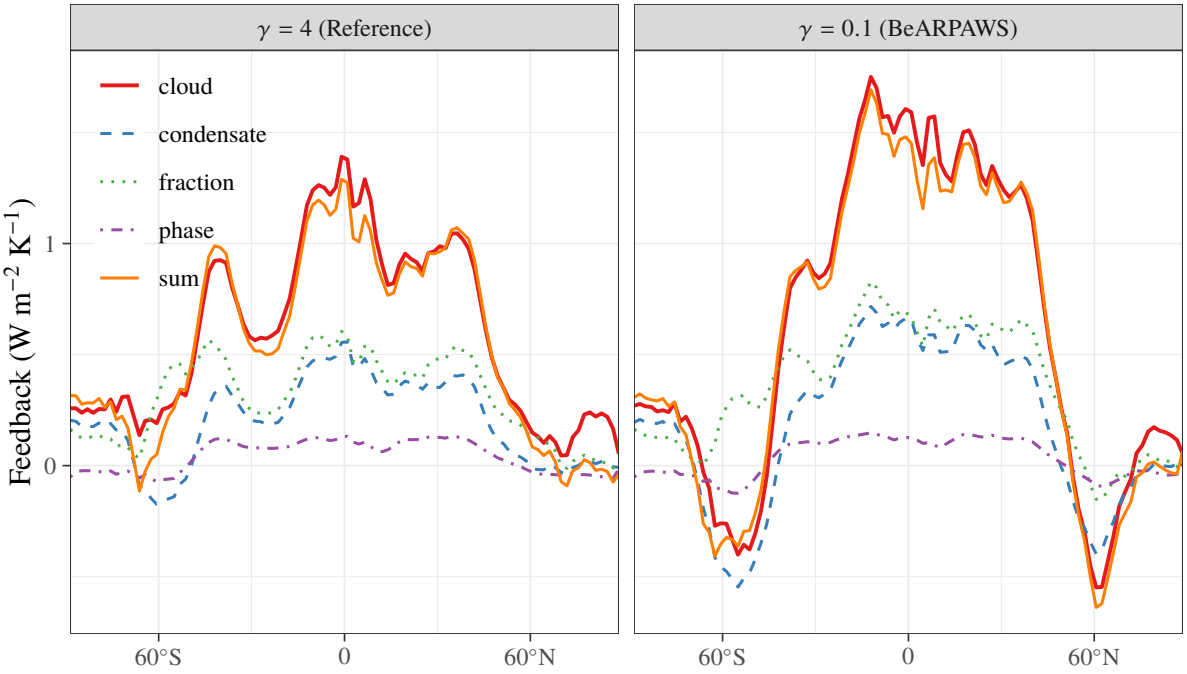

Supplementary Figure 5: Decomposition of the cloud feedback into components. The thick solid line is the PRP result for the total cloud feedback, while the thin solid line is the sum of the PRP results for individual components (fractional cover, condensate path, and phase).

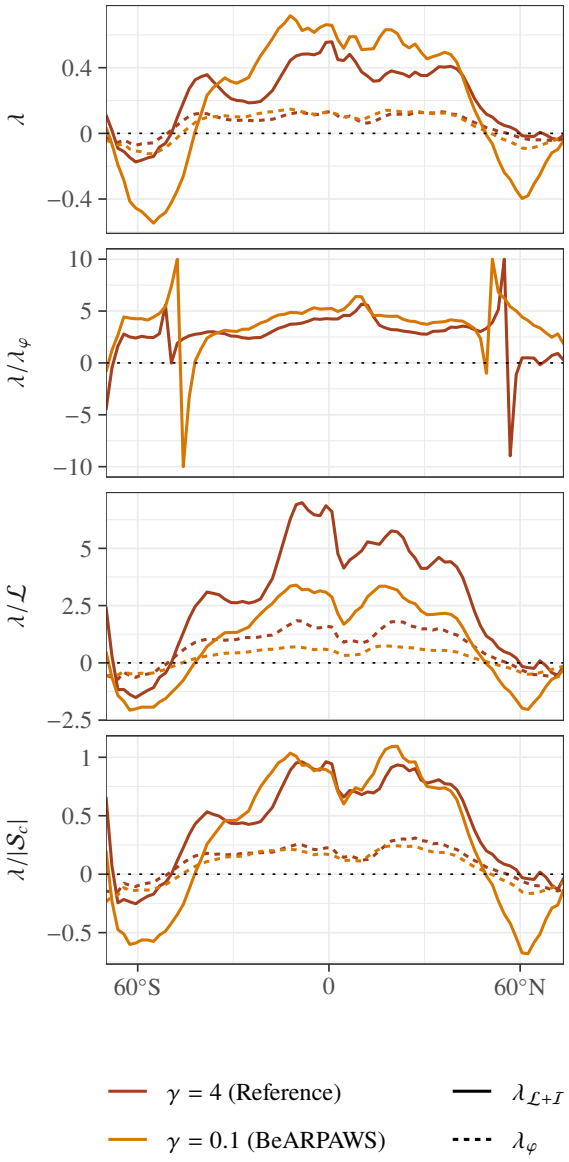

Supplementary Figure 6: Normalized feedback changes. The change in λ_φ and $\lambda_{\mathcal{L}+\mathcal{I}}$ is shown relative to other changes between the reference and reduced autconversion (BeARPAWS) model configurations. The units are $[\lambda] = \mathrm{W\,m^{-2}\,K^{-1}}$, $[\lambda/|\mathcal{S}_c|] = \%\,\mathrm{K^{-1}}$, and $[\lambda/\mathcal{L}] = \mathrm{W\,K^{-1}\,kg^{-1}}$.

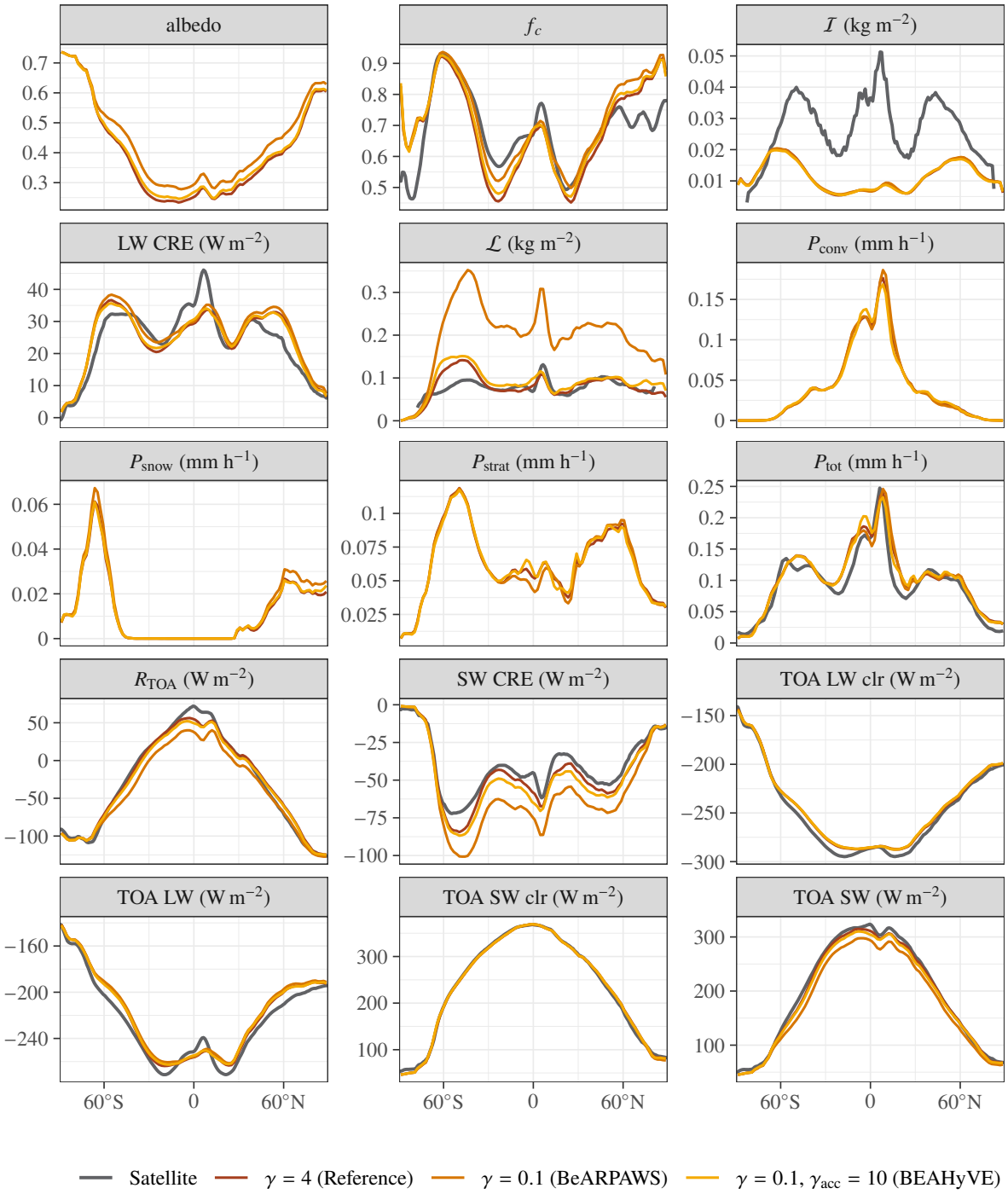

Supplementary Figure 7: Atmospheric state variables in various model configurations. Reference, reduced autconversion (BeARPAWS), and reduced autoconversion–increased accretion (BEAHyVE) are shown. Satellite datasets are as in Supplementary Figure 3.

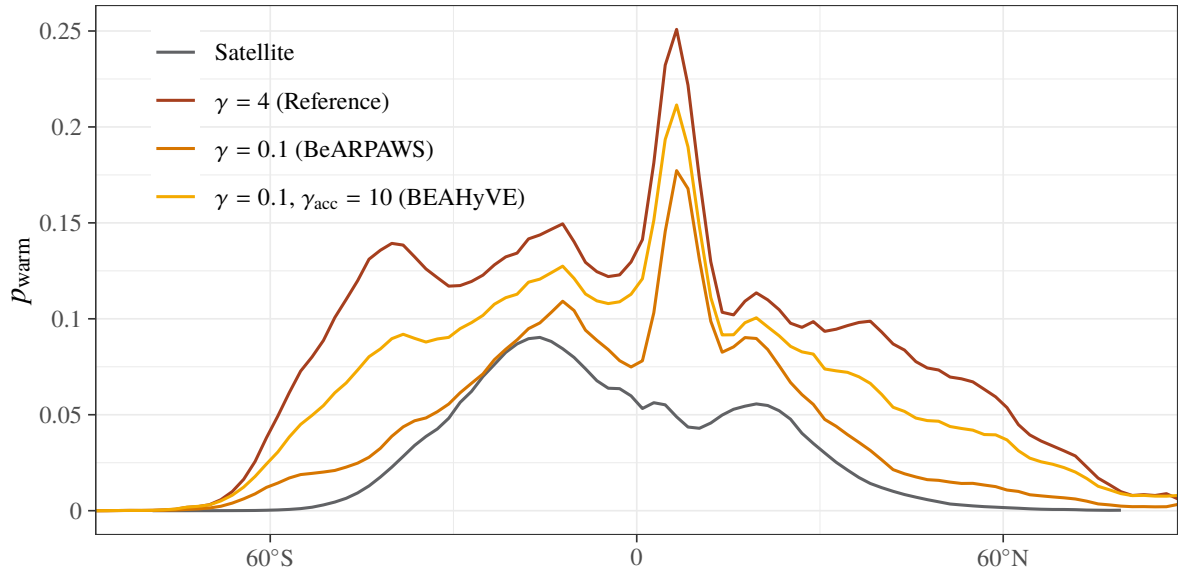

Supplementary Figure 8: Warm rain probability p_{warm}. The CloudSat–CALIPSO satellite climatology[40] and reference, reduced autconversion (BeARPAWS), and reduced autoconversion–increased accretion (BEAHyVE) model configurations are shown.

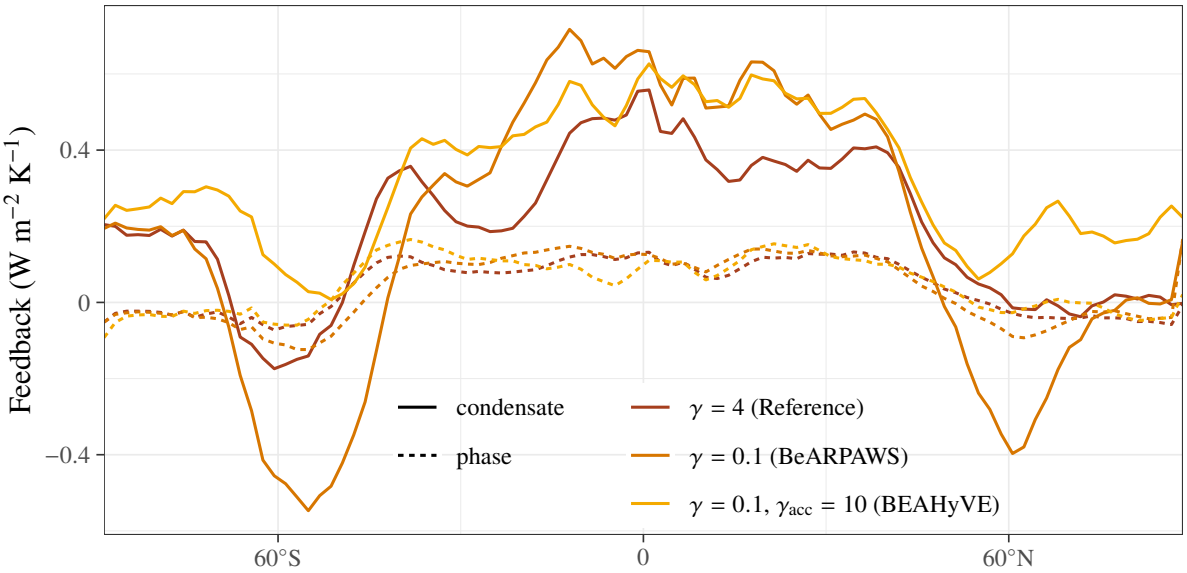

Supplementary Figure 9: Zonal-mean feedback components. The reference, reduced autconversion (BeARPAWS), and reduced autoconversion–increased accretion (BEAHyVE) configurations are shown.

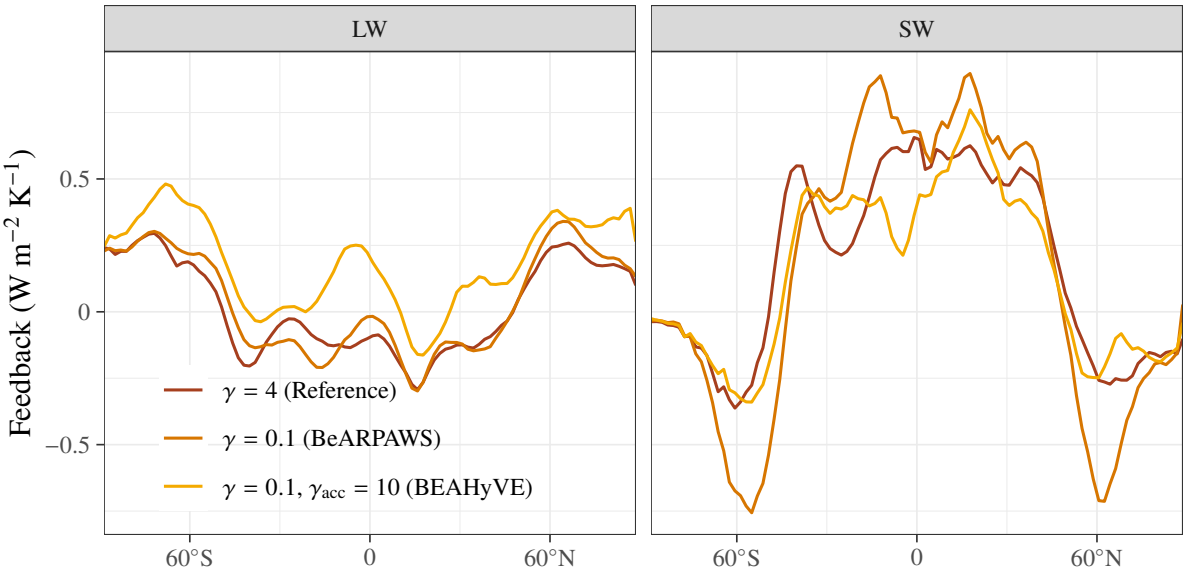

Supplementary Figure 10: Zonal-mean $\lambda_{\mathcal{L}+\mathcal{I}}$ feedback. The longwave (LW) and shortwave (SW) spectral components of the feedback are shown in the reference, reduced autconversion (BeARPAWS), and reduced autoconversion–increased accretion (BEAHyVE) configurations.

Supplementary Table 1: Results of background-subtracted feedback component fits. Global, northern hemisphere (NH), and southern hemisphere (SH) results in the reference and reduced autconversion (BeARPAWS) model configurations are shown.

	λ_ℓ (W m^{-2} K^{-1})			λ_o (W m^{-2} K^{-1})		
Model configuration	Global	NH	SH	Global	NH	SH
$\gamma = 4$ (Reference)	-0.059 ± 0.015	-0.032 ± 0.012	-0.028 ± 0.009	-0.025 ± 0.005	-0.014 ± 0.004	-0.011 ± 0.003
$\gamma = 0.1$ (BeARPAWS)	-0.171 ± 0.018	-0.078 ± 0.009	-0.093 ± 0.016	-0.041 ± 0.004	-0.020 ± 0.003	-0.021 ± 0.003

Supplementary Table 2: Present-day model state. Global means of state variables in the reference and reduced autconversion (BeARPAWS) model configurations are shown.

Model configuration	P (W m^{-2})	R_TOA (W m^{-2})	$\mathcal{S}_c$ (W m^{-2})	$\mathcal{L}$ (g m^{-2})
$\gamma = 4$ (Reference)	86.44	-0.13	-51.83	86
$\gamma = 0.1$ (BeARPAWS)	85.96	-13.94	-67.18	222

Supplementary Table 3: Feedback components. The PRP result for the total cloud feedback is indicated by "cloud", while "sum" is the sum of the PRP results for individual components (fractional cover, condensate path, and phase).

	Global-mean PRP estimate (W m^{-2} K^{-1})	
PRP perturbation	$\gamma = 4$ (Reference)	$\gamma = 0.1$ (BeARPAWS)
cloud	0.76	0.86
condensate	0.26	0.28
fraction	0.38	0.46
phase	0.07	0.07
sum	0.71	0.81

Supplementary Table 4: Normalized feedback strengths. The units are $[\lambda] = \mathrm{W\,m^{-2}\,K^{-1}}$, $[\lambda/\mathcal{S}_c] = \%\,\mathrm{K^{-1}}$, and $[\lambda/\mathcal{L}] = \mathrm{W\,K^{-1}\,kg^{-1}}$. Unprimed variables are taken from the reference model configuration, primed variables from the reduced autconversion (BeARPAWS) configuration.

χ	λ_ℓ/χ	λ'_ℓ/χ'	$(\lambda'_\ell/\chi')/(\lambda_\ell/\chi)$	λ_o/χ	$\lambda'_\mathrm{o}/\chi'$	$(\lambda_\mathrm{o}/\chi)/(\lambda'_\mathrm{o}/\chi')$
1	−0.059	−0.171	2.872	−0.025	−0.041	1.657
$\lvert\mathcal{S}_c\rvert$	−0.096	−0.228	2.371	−0.040	−0.055	1.369
λ_o	2.397	4.153	1.733	–	–	–
$\mathcal{L}$	−0.556	−0.701	1.261	−0.232	−0.169	0.728